

---

# Generalized Jensen-Shannon Divergence Loss for Learning with Noisy Labels

---

**Erik Englesson**

Division of Robotics, Perception and Learning  
KTH  
Stockholm, Sweden  
engless@kth.se

**Hossein Azizpour**

Division of Robotics, Perception and Learning  
KTH  
Stockholm, Sweden  
azizpour@kth.se

## Abstract

Prior works have found it beneficial to combine provably noise-robust loss functions *e.g.*, mean absolute error (MAE) with standard categorical loss function *e.g.*, cross entropy (CE) to improve their learnability. Here, we propose to use Jensen-Shannon divergence as a noise-robust loss function and show that it interestingly interpolate between CE and MAE with a controllable mixing parameter. Furthermore, we make a crucial observation that CE exhibit lower consistency around noisy data points. Based on this observation, we adopt a generalized version of the Jensen-Shannon divergence for multiple distributions to encourage consistency around data points. Using this loss function, we show state-of-the-art results on both synthetic (CIFAR), and real-world (WebVision) noise with varying noise rates.

## 1 Introduction

Labelled datasets, even the systematically annotated ones, contain noisy labels [1]. Therefore, designing noise-robust learning algorithms are crucial for the real-world tasks. An important avenue to tackle noisy labels is to devise noise-robust loss functions [2, 3, 4, 5]. Similarly, in this work, we propose two new noise-robust loss functions based on two central observations as follows.

Observation I: *Provably-robust loss functions can underfit the training data* [2, 3, 4, 5].

Observation II: *Standard networks show low consistency around noisy data points*, see Figure 1.

We first propose to use Jensen-Shannon divergence (JS) as a loss function which we crucially show interpolates between the noise-robust mean absolute error (MAE) and the cross entropy (CE) that better fits the data through faster convergence. Figure 2 illustrates the CE-MAE interpolation. Then, regarding the second observation, we adopt the generalized version of Jensen-Shannon divergence (GJS) to encourage consistency of the predictions, see Figure 3. Notably, Jensen-Shannon divergence has previously shown promise for test-time robustness to domain shift [6], here we further argue for its *training-time* robustness to *label noise*. The key contributions of this work are:

- we make a novel observation that a network predictions’ consistency is reduced for noisy-labelled data when overfitting to noise, which motivates the use of consistency regularization.
- We propose using Jensen-Shannon divergence (JS) and its multi-distribution generalization (GJS) as loss functions for learning with noisy labels. We relate JS to loss functions that are based on the noise-robustness theory of Ghosh *et al.* [2]. In particular, we prove that JS generalizes CE and MAE. Furthermore, we prove that GJS generalizes JS by incorporating consistency regularization in a single principled loss function.
- we provide an extensive set of empirical evidences on several datasets, noise types and rates. They show state-of-the-art results and give in-depth studies of the proposed losses.

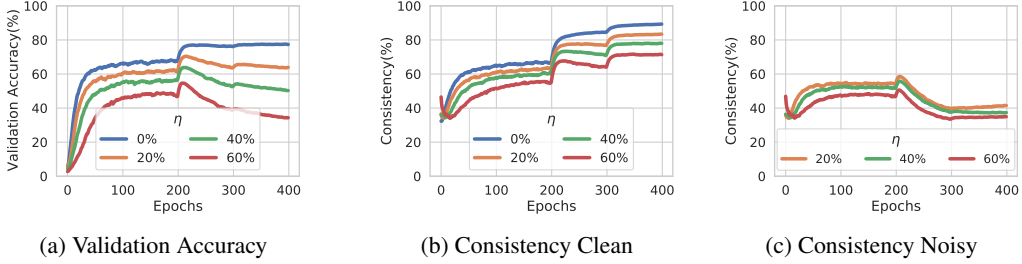


Figure 1: **Evolution of a trained network’s consistency as it overfits to noise using CE loss.** Here we plot the evolution of the validation accuracy (a) and network’s consistency (as measured by GJS) on clean (b) and noisy (c) examples of the training set of CIFAR-100 for varying symmetric noise rates when learning with the cross-entropy loss. The consistency of the learnt function and the accuracy closely correlate. Assuming causation, suggests that enforcing consistency may help avoid fitting to noise. Furthermore, the consistency is degraded more significantly for the noisy data points.

## 2 Generalized Jensen-Shannon Divergence

We propose two loss functions, the Jensen-Shannon divergence (JS) and its multi-distribution generalization (GJS). In this section, we first provide background and two observations that motivates our proposed loss functions. This is followed by definitions of the losses, and then we show that JS generalizes CE and MAE similar to other robust loss functions. Finally, we show how GJS generalizes JS to incorporate consistency regularization into a single principled loss function. We provide proofs of all theorems, propositions and remarks in this section in Appendix C.

### 2.1 Background & Motivation

**Supervised Classification.** Assume a general function class<sup>1</sup>  $\mathcal{F}$  where each  $f \in \mathcal{F}$  maps an input  $\mathbf{x} \in \mathbb{X} \rightarrow \Delta^{K-1}$ , i.e. a categorical distribution over  $K$  classes  $y \in \mathbb{Y} = \{1, 2, \dots, K\}$ . In supervised classification, we seek  $f^*$  that minimizes a risk  $R_{\mathcal{L}}(f) = \mathbb{E}_{\mathcal{D}}[\mathcal{L}(\mathbf{e}^{(y)}, f(\mathbf{x}))]$ , for some loss function  $\mathcal{L}$  and joint distribution  $\mathcal{D}$  over  $\mathbb{X} \times \mathbb{Y}$ , where  $\mathbf{e}^{(y)}$  is a  $K$ -vector with one at index  $y$  and zero elsewhere. In practice,  $\mathcal{D}$  is unknown and, instead, we use  $\mathcal{S} = \{(\mathbf{x}_i, y_i)\}_{i=1}^N$  which are independently sampled from  $\mathcal{D}$  to minimize an empirical risk  $\frac{1}{N} \sum_{i=1}^N \mathcal{L}(\mathbf{e}^{(y_i)}, f(\mathbf{x}_i))$ .

**Learning with Noisy Labels.** In this work, the goal is to learn from a noisy training distribution  $\mathcal{D}_{\eta}$  where the labels are changed, with probability  $\eta$ , from their true distribution  $\mathcal{D}$ . The noise is called *symmetric* if the noisy label is independent of the true label and *asymmetric* if it is class dependent. Let  $f_{\eta}^*$  be the optimizer of the noisy distribution risk  $R_{\mathcal{L}}^{\eta}(f)$ . A loss function  $\mathcal{L}$  is then called *robust* if  $f_{\eta}^*$  also minimizes  $R_{\mathcal{L}}$ . The MAE loss ( $\mathcal{L}_{MAE}(\mathbf{e}^{(y)}, f(\mathbf{x})) := \|\mathbf{e}^{(y)} - f(\mathbf{x})\|_1$ ) is robust but not CE [2].

**Issue of Underfitting.** Several works propose such robust loss functions and demonstrate their efficacy in preventing noise fitting [2, 3, 4, 5]. However, all those works have observed slow convergence of such robust loss functions leading to underfitting. This can be contrasted with CE that has fast convergence but overfits to noise. Ghosh *et al.* [2] mentions slow convergence of MAE and GCE [3] extensively analyzes the undefitting thereof. SCE [4] reports similar problems for the reverse cross entropy and proposes a linear combination with CE. Finally, Ma *et al.* [5] observe the same problem and consider combination of “active” and “passive” loss functions.

**Consistency Regularization.** This encourages a network to have consistent predictions for different perturbations of the same image, which has mainly been used for semi-supervised learning [7].

**Motivation.** In Figure 1, we show the validation accuracy and a measure of consistency during training with the CE loss for varying amounts of noise. First, we note that training with CE loss eventually overfits to noisy labels. Figure 1a, indicates that the higher the noise rate, the more accuracy drop when it starts to overfit to noise. Figure 1(b-c) shows the consistency of predictions for correct and noisy labelled examples of the training set, with consistency measured as the ratio of examples that have the same class prediction for two permutations of the same image, see Appendix B.4 for

<sup>1</sup>e.g. softmax neural network classifiers in this work

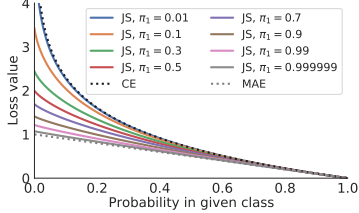


**Figure 2: JS interpolates between CE and MAE.** The Jensen-Shannon divergence (JS) for different values of  $\pi_1$ . The JS loss generalizes CE and MAE. For low values of the hyperparameter  $\pi_1$ , JS behaves like CE and for increasing values of  $\pi_1$  it behaves more like the noise robust MAE loss.

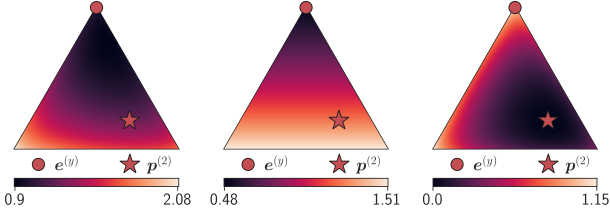


**Figure 3: GJS Dissection for M=K=3:** The decomposition of  $\mathcal{L}_{\text{GJS}}$  (left) into a JS term (middle) and a consistency term (right) from Proposition 2. Each point in the simplex correspond to a  $\mathbf{p}^{(3)} \in \Delta^2$ , where the color represents the value of the loss at that point. It can be seen that there are two ways to minimize  $\mathcal{L}_{\text{GJS}}$ , either by making the predictions similar to the label (middle) or similar to the other predictions (right) to increase consistency. To better highlight the variations of the losses, each loss has its own range of values.

more details. A clear correlation is observed between accuracy and consistency of the noisy examples. Assuming causality, suggests that maximizing consistency of predictions may improve robustness to noise. Next, we define simple loss functions that (i) encourage consistency around data points and (ii) alleviate the “issue of underfitting” by interpolating between CE and MAE.

## 2.2 Definitions

**$D_{\text{JS}}$ .** Let  $\mathbf{p}^{(1)}, \mathbf{p}^{(2)} \in \Delta^{K-1}$  have corresponding weights  $\boldsymbol{\pi} = [\pi_1, \pi_2]^T \in \Delta$ . Then, the Jensen-Shannon divergence between  $\mathbf{p}^{(1)}$  and  $\mathbf{p}^{(2)}$  is

$$D_{\text{JS}, \boldsymbol{\pi}}(\mathbf{p}^{(1)}, \mathbf{p}^{(2)}) := H(\mathbf{m}) - \pi_1 H(\mathbf{p}^{(1)}) - \pi_2 H(\mathbf{p}^{(2)}) = \pi_1 D_{\text{KL}}(\mathbf{p}^{(1)} \parallel \mathbf{m}) + \pi_2 D_{\text{KL}}(\mathbf{p}^{(2)} \parallel \mathbf{m}) \quad (1)$$

with  $H$  the Shannon entropy, and  $\mathbf{m} = \pi_1 \mathbf{p}^{(1)} + \pi_2 \mathbf{p}^{(2)}$ . Unlike Kullback–Leibler divergence ( $D_{\text{KL}}(\mathbf{p}^{(1)} \parallel \mathbf{p}^{(2)})$ ) or cross entropy (CE), JS is symmetric, does not require absolute continuity, and is bounded. As we will see later, the weighting mechanism ( $\boldsymbol{\pi}$ ) is another crucial difference.

**$D_{\text{GJS}}$ .** Similar to  $D_{\text{KL}}$ ,  $D_{\text{JS}}$  satisfies  $D_{\text{JS}, \boldsymbol{\pi}}(\mathbf{p}^{(1)}, \mathbf{p}^{(2)}) \geq 0$ , with equality iff  $\mathbf{p}^{(1)} = \mathbf{p}^{(2)}$ . For  $D_{\text{JS}}$ , this is derived from Jensen’s inequality for the concave Shannon entropy. This property holds for finite number of distributions and motivates a generalization of  $D_{\text{JS}}$  to multiple distributions:

$$D_{\text{GJS}, \boldsymbol{\pi}}(\mathbf{p}^{(1)}, \dots, \mathbf{p}^{(M)}) := H\left(\sum_{i=1}^M \pi_i \mathbf{p}^{(i)}\right) - \sum_{i=1}^M \pi_i H(\mathbf{p}^{(i)}) = \sum_{i=1}^M \pi_i D_{\text{KL}}\left(\mathbf{p}^{(i)} \parallel \sum_{j=1}^M \pi_j \mathbf{p}^{(j)}\right) \quad (2)$$

where  $M$  is the number of distributions, and  $\boldsymbol{\pi} = [\pi_1, \dots, \pi_M]^T \in \Delta^{M-1}$ .

**Loss functions.** We aim to use  $D_{\text{JS}}$  and  $D_{\text{GJS}}$  divergences, to measure deviation of the predictive distribution(s),  $f(\mathbf{x})$ , from the target distribution,  $e^{(y)}$ . Without loss of generality, hereafter, we dedicate  $\mathbf{p}^{(1)}$  to denote the target distribution. JS loss, therefore, can take the form of  $D_{\text{JS}, \boldsymbol{\pi}}(e^{(y)}, f(\mathbf{x}))$ . Generalized JS loss is a less straight-forward construction since  $D_{\text{GJS}}$  can accommodate more predictive distributions. While various choices can be made for these distributions, in this work, we consider predictions associated with different random perturbations of a sample, denoted by  $\mathcal{A}(\mathbf{x})$ . This choice, as shown later, implies an interesting analogy to *consistency regularization*. The choice, also, entails no distinction between the  $M-1$  predictive distributions. Therefore, we consider  $\pi_2 = \dots = \pi_M = \frac{1-\pi_1}{M-1}$  in all our experiments. Finally, we scale the loss functions by a constant factor  $Z = -(1-\pi_1) \log(1-\pi_1)$ . This seemingly-arbitrary scaling does not affect the behavior of the loss but, as we will see later, makes the analytical presentation of the theoretical statements simpler. Formally, we have JS and GJS losses:

$$\mathcal{L}_{\text{JS}}(y, f, \mathbf{x}) := \frac{D_{\text{JS}, \boldsymbol{\pi}}(e^{(y)}, f(\mathbf{x}))}{Z}, \quad \mathcal{L}_{\text{GJS}}(y, f, \mathbf{x}) := \frac{D_{\text{GJS}, \boldsymbol{\pi}}(e^{(y)}, f(\tilde{\mathbf{x}}^{(2)}), \dots, f(\tilde{\mathbf{x}}^{(M)}))}{Z} \quad (3)$$

with  $\tilde{\mathbf{x}}^{(i)} \sim \mathcal{A}(\mathbf{x})$ . Next, we study the connection between JS and losses which are based on the robustness theory of Ghosh *et al.* [2].

### 2.3 JS's Connection to Robust Losses

Cross Entropy (CE) is the prevalent loss function for deep classifiers with remarkable successes. However, CE is prone to fitting noise [8]. On the other hand, Mean Absolute Error (MAE) is theoretically noise-robust [2]. Evidently, standard optimization algorithms struggle to minimize MAE, especially for more challenging datasets *e.g.* CIFAR-100 [3, 5]. Therefore, there have been several proposals that combine CE and MAE, such as GCE [3], SCE [4], and NCE+MAE [5]. The rationale is for CE to help with the learning dynamics of MAE. Next, we show JS has CE and MAE as its asymptotes w.r.t.  $\pi_1$ .

**Proposition 1.** *Let  $\mathbf{p} \in \Delta^{K-1}$ , then*

$$\lim_{\pi_1 \rightarrow 0} \mathcal{L}_{\text{JS}}(\mathbf{e}^{(y)}, \mathbf{p}) = H(\mathbf{e}^{(y)}, \mathbf{p}), \quad \lim_{\pi_1 \rightarrow 1} \mathcal{L}_{\text{JS}}(\mathbf{e}^{(y)}, \mathbf{p}) = \frac{1}{2} \|\mathbf{e}^{(y)} - \mathbf{p}\|_1 \quad (4)$$

where  $H(\mathbf{e}^{(y)}, \mathbf{p})$  is the cross entropy of  $\mathbf{e}^{(y)}$  relative to  $\mathbf{p}$ .

Figure 2 depicts how JS interpolates between CE and MAE asymptotes for  $\pi_1 \in (0, 1)$ . The proposition reveals an interesting connection to state-of-the-art robust loss functions, however, there are important differences. SCE is not bounded (so it cannot be used in Theorem 1), and GCE is not symmetric, while JS and MAE are both symmetric and bounded. In Appendix B.1, we perform a dissection to better understand how these properties affect learning with noisy labels. GCE is most similar to JS and is compared further in Appendix B.3.

A crucial difference to these other losses is that JS naturally extends to multiple predictive distributions (GJS). Next, we show how GJS generalizes JS by incorporating consistency regularization.

### 2.4 GJS's Connection to Consistency Regularization

In Figure 1, it was shown how the consistency of the noisy labelled examples was reduced when the network overfitted to noise. The following proposition shows how GJS naturally encourages consistency in a single principled loss function.

**Proposition 2.** *Let  $\mathbf{p}^{(2)}, \dots, \mathbf{p}^{(M)} \in \Delta^{K-1}$  with  $M \geq 3$  and  $\mathbf{m}_{>1} = \frac{\sum_{j=2}^M \pi_j \mathbf{p}^{(j)}}{1-\pi_1}$ , then*

$$\mathcal{L}_{\text{GJS}}(\mathbf{e}^{(y)}, \mathbf{p}^{(2)}, \dots, \mathbf{p}^{(M)}) = \mathcal{L}_{\text{JS}_{\pi'}}(\mathbf{e}^{(y)}, \mathbf{m}_{>1}) + (1 - \pi_1) \mathcal{L}_{\text{GJS}_{\pi''}}(\mathbf{p}^{(2)}, \dots, \mathbf{p}^{(M)})$$

where  $\pi' = [\pi_1, 1 - \pi_1]^T$  and  $\pi'' = \frac{[\pi_2, \dots, \pi_M]^T}{(1 - \pi_1)}$ .

Importantly, Proposition 2 shows that GJS can be decomposed into two terms: 1) a JS term between the label and the mean prediction  $\mathbf{m}_{>1}$ , and 2) a GJS term, but without the label. Figure 3 illustrates the effect of this decomposition. The first term, similarly to the standard JS loss, encourages the predictions' mean to be closer to the label (Figure 3 middle). However, the second term encourages all the predictions to be similar, that is, *consistency regularization* (Figure 3 right).

### 2.5 Noise Robustness

Here, the robustness properties of JS and GJS are analyzed in terms of lower ( $B_L$ ) and upper bounds ( $B_U$ ) for the following theorem, which generalizes the results by Zhang *et al.* [3] to any bounded loss function, even with multiple predictive distributions.

**Theorem 1.** *Under symmetric noise with  $\eta < \frac{K-1}{K}$ , if  $B_L \leq \sum_{i=1}^K \mathcal{L}(\mathbf{e}^{(i)}, \mathbf{x}, f) \leq B_U, \forall \mathbf{x}, f$  is satisfied for a loss  $\mathcal{L}$ , then*

$$0 \leq R_{\mathcal{L}}^{\eta}(f^*) - R_{\mathcal{L}}^{\eta}(f_{\eta}^*) \leq \eta \frac{B_U - B_L}{K-1}, \quad \text{and} \quad -\frac{\eta(B_U - B_L)}{K-1 - \eta K} \leq R_{\mathcal{L}}(f^*) - R_{\mathcal{L}}(f_{\eta}^*) \leq 0, \quad (5)$$

A tighter bound  $B_U - B_L$ , implies a smaller worst case risk difference of the optimal classifiers (robust when  $B_U = B_L$ ). Importantly, while  $\mathcal{L}(\mathbf{e}^{(i)}, \mathbf{x}, f) = \mathcal{L}(\mathbf{e}^{(i)}, f(\mathbf{x}))$  usually, this subtle distinction is useful for losses with multiple predictive distributions, see Equation 3.

For losses with multiple predictive distributions, the bounds in Theorem 1 must hold for any  $\mathbf{x}$  and  $f$ , *i.e.*, for any combination of  $M - 1$  categorical distributions on  $K$  classes. The following proposition provides such bounds for GJS.

**Proposition 3.** GJS loss with  $M \leq K + 1$  satisfies  $B_L \leq \sum_{k=1}^K \mathcal{L}_{\text{GJS}}(\mathbf{e}^{(k)}, \mathbf{p}^{(2)}, \dots, \mathbf{p}^{(M)}) \leq B_U$  for all  $\mathbf{p}^{(2)}, \dots, \mathbf{p}^{(M)} \in \Delta^{K-1}$ , with the following bounds

$$B_L = \sum_{k=1}^K \mathcal{L}_{\text{GJS}}(\mathbf{e}^{(k)}, \mathbf{u}, \dots, \mathbf{u}), \quad B_U = \sum_{k=1}^K \mathcal{L}_{\text{GJS}}(\mathbf{e}^{(k)}, \mathbf{e}^{(1)}, \dots, \mathbf{e}^{(M-1)}) \quad (6)$$

Note, the bounds for JS is a special case of Proposition 3 for  $M = 2$ .

**Remark 1.**  $\mathcal{L}_{\text{JS}}$  and  $\mathcal{L}_{\text{GJS}}$  are robust ( $B_L = B_U$ ) in the limit of  $\pi_1 \rightarrow 1$ .

Remark 1 is intuitive from Section 2.3 which showed that  $\mathcal{L}_{\text{JS}}$  is equivalent to the robust MAE in this limit and that the consistency term in Proposition 2 vanishes. In Appendix C.1, we further prove robustness of the proposed losses to asymmetric noise.

### 3 Related Works

Interleaved in the previous sections we covered most-related works to us, *i.e.* the avenue of identification or construction of *theoretically-motivated robust loss functions* [2, 3, 4, 5]. These works, similar to this paper, follow the theoretical construction of Ghosh *et al.* [2]. Furthermore, Liu&Guo [9] use “peer prediction” to propose a new family of robust loss functions. Different to these works, here, we propose loss functions based on  $D_{\text{JS}}$  which holds various desirable properties of those prior works while exhibiting novel ties to consistency regularization; a recent important regularization technique.

Next, we briefly cover other lines of work. A more thorough version can be found in Appendix D.

A direction, that similar to us does not alter training, *reweight a loss function* by confusion matrix [10, 11, 12, 13, 14]. Assuming a class-conditional noise model, loss correction is theoretically motivated and perfectly orthogonal to noise-robust losses.

*Consistency regularization* is a recent technique that imposes smoothness in the learnt function for semi-supervised learning [7] and recently for noisy data [15]. These works use different complex pipelines for such regularization. GJS encourages consistency in a simple way that exhibits other desirable properties for learning with noisy labels. Importantly, Hendrycks *et al.* [6] used Jensen-Shannon-based loss functions to improve test-time robustness to image corruptions which further verifies the general usefulness of GJS. In this work, we study such loss functions for the different goal of *training-time label-noise robustness*. In this context, our thorough analytical and empirical results are, to the best of our knowledge, novel.

Recently, loss functions with *information-theoretic* motivations have been proposed [16, 17]. JS, with apparent information theoretic interpretation, has strong connection to those. Especially, the latter is a close concurrent work but takes a different and complementary angle. The connection of these works can be a fruitful future direction.

### 4 Experiments

This section, first, empirically investigates the effectiveness of the proposed losses for learning with noisy labels, on synthetic (Section 4.1) and real-world noise (Section 4.2). This is followed by several experiments and ablation studies (Section 4.3) to shed light on the properties of JS and GJS through empirical substantiation of the theories and claims provided in Section 2. All these additional experiments are done on the more challenging CIFAR-100 dataset.

**Experimental Setup.** We use ResNet 34 and 50 for experiments on CIFAR and WebVision datasets respectively and optimize them using SGD with momentum. The complete details of the training setup can be found in Appendix A. Most importantly, we take three main measures to ensure a fair and reliable comparison throughout the experiments: 1) we reimplement all the loss functions we compare with in a single shared learning setup, 2) we use the same hyperparameter optimization budget and mechanism for all the prior works and ours, and 3) we train and evaluate five networks for individual results, where in each run the synthetic noise, network initialization, and data-order are differently randomized. The thorough analysis is evident from the higher performance of CE in our setup compared to prior works. Where possible, we report mean and standard deviation and denote the statistically-significant top performers with student t-test.

Table 1: **Synthetic Noise Benchmark on CIFAR.** We reimplement other noise-robust loss functions into the *same learning setup* and ResNet-34, including label smoothing (LS), Bootstrap (BS), Symmetric CE (SCE), Generalized CE (GCE), and Normalized CE (NCE+RCE). We used *same hyperparameter optimization budget and mechanism* for all the prior works and ours. Mean test accuracy and standard deviation are reported from five runs and the statistically-significant top performers are boldfaced. The thorough analysis is evident from the higher performance of CE in our setup compared to prior works. GJS achieves state-of-the-art results for different noise rates, types, and datasets. Generally, GJS’s efficacy is more evident for the more challenging CIFAR-100 dataset.

Dataset	Method	No Noise		Symmetric Noise Rate				Asymmetric Noise Rate	
		0%	20%	40%	60%	80%	20%	40%	
CIFAR-10	CE	<b>95.77</b> $\pm$ <b>0.11</b>	91.63 $\pm$ 0.27	87.74 $\pm$ 0.46	81.99 $\pm$ 0.56	66.51 $\pm$ 1.49	92.77 $\pm$ 0.24	87.12 $\pm$ 1.21	
	BS	94.58 $\pm$ 0.25	91.68 $\pm$ 0.32	89.23 $\pm$ 0.16	82.65 $\pm$ 0.57	16.97 $\pm$ 6.36	93.06 $\pm$ 0.25	88.87 $\pm$ 1.06	
	LS	95.64 $\pm$ 0.12	93.51 $\pm$ 0.20	89.90 $\pm$ 0.20	83.96 $\pm$ 0.58	67.35 $\pm$ 2.71	92.94 $\pm$ 0.17	88.10 $\pm$ 0.50	
	SCE	<b>95.75</b> $\pm$ <b>0.16</b>	94.29 $\pm$ 0.14	92.72 $\pm$ 0.25	89.26 $\pm$ 0.37	<b>80.68</b> $\pm$ <b>0.42</b>	93.48 $\pm$ 0.31	84.98 $\pm$ 0.76	
	GCE	<b>95.75</b> $\pm$ <b>0.14</b>	94.24 $\pm$ 0.18	92.82 $\pm$ 0.11	89.37 $\pm$ 0.27	<b>79.19</b> $\pm$ <b>2.04</b>	92.83 $\pm$ 0.36	87.00 $\pm$ 0.99	
	NCE+RCE	95.36 $\pm$ 0.09	94.27 $\pm$ 0.18	92.03 $\pm$ 0.31	87.30 $\pm$ 0.35	77.89 $\pm$ 0.61	<b>93.87</b> $\pm$ <b>0.03</b>	86.83 $\pm$ 0.84	
	JS	<b>95.89</b> $\pm$ <b>0.10</b>	94.52 $\pm$ 0.21	93.01 $\pm$ 0.22	89.64 $\pm$ 0.15	76.06 $\pm$ 0.85	92.18 $\pm$ 0.31	87.99 $\pm$ 0.55	
CIFAR-100	GJS	<b>95.91</b> $\pm$ <b>0.09</b>	<b>95.33</b> $\pm$ <b>0.18</b>	<b>93.57</b> $\pm$ <b>0.16</b>	<b>91.64</b> $\pm$ <b>0.22</b>	79.11 $\pm$ 0.31	<b>93.94</b> $\pm$ <b>0.25</b>	<b>89.65</b> $\pm$ <b>0.37</b>	
	CE	77.60 $\pm$ 0.17	65.74 $\pm$ 0.22	55.77 $\pm$ 0.83	44.42 $\pm$ 0.84	10.74 $\pm$ 4.08	66.85 $\pm$ 0.32	49.45 $\pm$ 0.37	
	BS	77.65 $\pm$ 0.29	72.92 $\pm$ 0.50	68.52 $\pm$ 0.54	53.80 $\pm$ 1.76	13.83 $\pm$ 4.41	73.79 $\pm$ 0.43	<b>64.67</b> $\pm$ <b>0.69</b>	
	LS	78.60 $\pm$ 0.04	74.88 $\pm$ 0.15	68.41 $\pm$ 0.20	54.58 $\pm$ 0.47	26.98 $\pm$ 1.07	73.17 $\pm$ 0.46	57.20 $\pm$ 0.85	
	SCE	78.29 $\pm$ 0.24	74.21 $\pm$ 0.37	68.23 $\pm$ 0.29	59.28 $\pm$ 0.58	26.80 $\pm$ 1.11	70.86 $\pm$ 0.44	51.12 $\pm$ 0.37	
	GCE	77.65 $\pm$ 0.17	75.02 $\pm$ 0.24	71.54 $\pm$ 0.39	65.21 $\pm$ 0.16	<b>49.68</b> $\pm$ <b>0.84</b>	72.13 $\pm$ 0.39	51.50 $\pm$ 0.71	
	NCE+RCE	74.66 $\pm$ 0.21	72.39 $\pm$ 0.24	68.79 $\pm$ 0.29	62.18 $\pm$ 0.35	31.63 $\pm$ 3.59	71.35 $\pm$ 0.16	57.80 $\pm$ 0.52	
	JS	77.95 $\pm$ 0.39	75.41 $\pm$ 0.28	71.12 $\pm$ 0.30	64.36 $\pm$ 0.34	45.05 $\pm$ 0.93	71.70 $\pm$ 0.36	49.36 $\pm$ 0.25	
	GJS	<b>79.27</b> $\pm$ <b>0.29</b>	<b>78.05</b> $\pm$ <b>0.25</b>	<b>75.71</b> $\pm$ <b>0.25</b>	<b>70.15</b> $\pm$ <b>0.30</b>	44.49 $\pm$ 0.53	<b>74.60</b> $\pm$ <b>0.47</b>	63.70 $\pm$ 0.22	

#### 4.1 Synthetic Noise Benchmarks: CIFAR

Here, we evaluate the proposed loss functions on the CIFAR datasets with two types of synthetic noise: symmetric and asymmetric. For symmetric noise, the labels are, with probability  $\eta$ , resampled from a uniform distribution over all labels. For asymmetric noise, we follow the standard setup of Patrini *et al.* [18]. For CIFAR-10, the labels are modified, with probability  $\eta$ , as follows: *truck*  $\rightarrow$  *automobile*, *bird*  $\rightarrow$  *airplane*, *cat*  $\leftrightarrow$  *dog*, and *deer*  $\rightarrow$  *horse*. For CIFAR-100, labels are, with probability  $\eta$ , cycled to the next sub-class of the same “super-class”, *e.g.* the labels of super-class “vehicles 1” are modified as follows: *bicycle*  $\rightarrow$  *bus*  $\rightarrow$  *motorcycle*  $\rightarrow$  *pickup truck*  $\rightarrow$  *bicycle*.

We compare with other noise-robust loss functions such as label smoothing (LS) [19], Bootstrap (BS) [20], Symmetric Cross-Entropy (SCE) [4], Generalized Cross-Entropy (GCE) [3], and the NCE+RCE loss of Ma *et al.* [5]. We do not compare to methods that propose a full pipeline since, first, a conclusive comparison would require re-implementation and individual evaluation of several components and second, robust loss functions can be considered complementary to them.

**Results.** Table 1 shows the results for symmetric and asymmetric noise on CIFAR-10 and CIFAR-100. GJS performs similarly or better than other methods for different noise rates, noise types, and data sets. Generally, GJS’s efficacy is more evident for the more challenging CIFAR-100 dataset. For example, on 60% uniform noise on CIFAR-100, the difference between GJS and the second best (GCE) is 4.94 percentage points while our results on 80% noise is lower than GCE. We attribute this to the high sensitivity of the results to the hyperparameter settings in such a high-noise rate which are also generally unrealistic (WebVision has  $\sim$ 20%). The performance of JS is consistently similar to the top performance of the prior works across different noise rates, types and datasets. In Section 4.3, we substantiate the importance of the consistency term, identified in Proposition 2, when going from JS to GJS that helps with the learning dynamics and reduce susceptibility to noise. Next, we test the proposed losses on a naturally-noisy dataset to see their efficacy in a real-world scenario.

#### 4.2 Real-World Noise Benchmark: WebVision

WebVision v1 is a large-scale image dataset collected by crawling Flickr and Google, which resulted in an estimated 20% of noisy labels [23]. There are 2.4 million images of the same thousand classes as ILSVRC12. Here, we use a smaller version called mini WebVision [24] consisting of the first 50 classes of the Google subset.

Table 2: **Real-world Noise Benchmark on WebVision.** Mean test accuracy and standard deviation from five runs are reported for the validation sets of (mini) WebVision and ILSVRC12. GJS with two networks correspond to the mean prediction of two independently trained GJS networks with different seeds for data augmentation and weight initialization. Here, GJS uses  $Z = 1$ . Results marked with  $\dagger$  are from Zheltonozhskii *et al.* [21].

Method	Architecture	Augmentation	Networks	WebVision		ILSVRC12	
				Top 1	Top 5	Top 1	Top 5
ELR+[22] $\dagger$	Inception-ResNet-V2	Mixup	2	77.78	<b>91.68</b>	70.29	89.76
DivideMix[15] $\dagger$	Inception-ResNet-V2	Mixup	2	77.32	<b>91.64</b>	<b>75.20</b>	90.84
DivideMix[15] $\dagger$	ResNet-50	Mixup	2	$76.32 \pm 0.36$	$90.65 \pm 0.16$	$74.42 \pm 0.29$	<b>91.21 <math>\pm 0.12</math></b>
CE	ResNet-50	ColorJitter	1	$70.69 \pm 0.66$	$88.64 \pm 0.17$	$67.32 \pm 0.57$	$88.00 \pm 0.49$
JS	ResNet-50	ColorJitter	1	$74.56 \pm 0.32$	$91.09 \pm 0.08$	$70.36 \pm 0.12$	$90.60 \pm 0.09$
GJS	ResNet-50	ColorJitter	1	$77.99 \pm 0.35$	$90.62 \pm 0.28$	$74.33 \pm 0.46$	$90.33 \pm 0.20$
GJS	ResNet-50	ColorJitter	2	<b>79.28 <math>\pm 0.24</math></b>	$91.22 \pm 0.30$	<b>75.50 <math>\pm 0.17</math></b>	<b>91.27 <math>\pm 0.26</math></b>

**Results.** Table 2, as the common practice, reports the performances on the validation sets of WebVision and ILSVRC12 (first 50 classes). Both JS and GJS exhibits large margins with standard CE, especially using top-1 accuracy. Top-5 accuracy, due to its admissibility of wrong top predictions, can obscure the susceptibility to noise-fitting and thus indicates smaller but still significant improvements.

The two state-of-the-art methods on this dataset were DivideMix[15] and ELR+[22]. Compared to our setup, both these methods use a stronger network (Inception-ResNet-V2 vs ResNet-50), stronger augmentations (Mixup vs color jittering) and co-train two networks. Furthermore, ELR+ uses an exponential moving average of weights and DivideMix treats clean and noisy labelled examples differently after separating them using Gaussian mixture models. Despite these differences, GJS performs as good or better in terms of top-1 accuracy on WebVision and significantly outperforms ELR+ on ILSVRC12 (70.29 vs 74.33). To show the importance of these differences, we add one of their components to GJS, *i.e.* the use of two networks. We train an ensemble of two independent networks with the GJS loss and average their predictions (last row of Table 2). This simple extension, which requires no change in the training code, gives significant improvements. To the best of our knowledge, this is the best reported top-1 accuracy on WebVision and ILSVRC12 when no pre-training is used.

So far, the experiments demonstrated the robustness of the proposed loss function (regarding Proposition 3) via the significant improvements of final accuracy on noisy datasets. While this was central and informative, it is also important to investigate whether this improvement come from the theoretical properties that were argued for JS and GJS. In what follows, we devise several such experiments, in an effort to substantiate the theoretical claims and conjectures.

### 4.3 Towards a Better Understanding of the Jensen-Shannon-based Loss Functions

Here, we study the behavior of the losses for different distribution weights  $\pi_1$ , number of distributions  $M$ , and epochs. We also provide insights on why GJS performs better than JS.

**How does  $\pi_1$  control the trade-off of robustness and learnability?** In Figure 4, we plot the validation accuracy during training for both JS and GJS at different values of  $\pi_1$  and noise rates  $\eta$ . From Proposition 1, we expect JS to behave as CE for low values of  $\pi_1$  and as MAE for larger values of  $\pi_1$ . Figure 4 (a-b) confirms this. Specifically,  $\pi_1 = 0.1$  learns quickly and performs well for low noise but overfits for  $\eta = 0.6$  (characteristic of non-robust CE), on the other hand,  $\pi_1 = 0.9$  learns slowly but is robust to high noise rates (characteristic of noise-robust MAE).

In Figure 4 (c-d), we observe two qualitative differences between GJS and JS: 1) GJS helps the learning dynamics for larger values of  $\pi_1$  that otherwise learns slowly, and 2) converges to a higher validation accuracy.

**How many distributions to use?** Figure 5 depicts validation accuracy for varying number of distributions  $M$ . For all noise rates, we observe a performance increase going from  $M = 2$  to  $M = 3$ . However, the performance of  $M > 3$  depends on the noise rate. For lower noise rates, having more than three distributions can improve the performance. For higher noise rates *e.g.* 60%, having  $M > 3$  degrades the performance. For simplicity, we have used  $M = 3$  for all experiments with GJS.

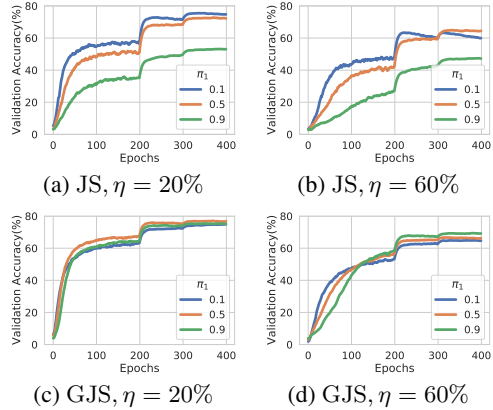


Figure 4: **Effect of  $\pi_1$ .** Validation accuracy of JS and GJS during training with symmetric noise on CIFAR100. From Proposition 1, JS behaves like CE and MAE for low and high values of  $\pi_1$ , respectively. The signs of noise-fitting for  $\pi_1 = 0.1$  on 60% noise (b), and slow learning of  $\pi_1 = 0.9$  (a-b), show this in practice. The GJS loss does not exhibit overfitting for low values of  $\pi_1$  and learns quickly for large values of  $\pi_1$  (c-d).

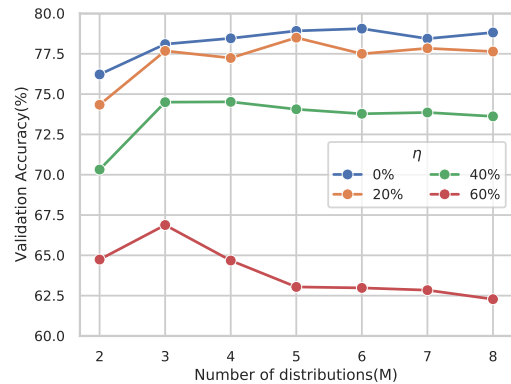


Figure 5: **Effect of  $M$ .** Validation accuracy for increasing number of distributions ( $M$ ) and different symmetric noise rates on CIFAR-100 with  $\pi_1 = \frac{1}{2}$ . For all noise rates, using three instead of two distributions results in a higher accuracy. Going beyond three distributions is only helpful for lower noise rates. For simplicity we use  $M = 3$  (corresponding to two augmentations) for all of our experiments.

**Is the improvements of GJS over JS due to mean prediction or consistency?** Proposition 2 decomposed GJS into a JS term with a mean prediction ( $\mathbf{m}_{>1}$ ) and a consistency term operating on all distributions but the target. In Table 3, we compare the performance of JS and GJS to GJS without the consistency term, i.e.,  $\mathcal{L}_{JS_{\pi'}}(e^{(y)}, \mathbf{m}_{>1})$ . The results suggest that the improvement of GJS over JS can be attributed to the consistency term.

Figure 4 (a-b) showed that JS improves the learning dynamics of MAE by blending it with CE, controlled by  $\pi_1$ . Similarly, we see here that the consistency term also improves the learning dynamics (underfitting and convergence speed) of MAE. Interestingly, Figure 4 (c-d), shows the higher values of  $\pi_1$  (closer to MAE) works best for GJS, hinting that, the consistency term improves the learning dynamics of MAE so much so that the role of CE becomes less important.

**Is GJS mostly helping the clean or noisy examples?** To better understand the improvements of GJS over JS, we perform an ablation with different losses for clean and noisy examples, see Table 4. We observe that using GJS instead of JS improves performance in all cases. Importantly, using GJS only for the noisy examples performs significantly better than only using it for the clean examples (74.1 vs 72.9). The best result is achieved when using GJS for both clean and noisy examples but still close to the noisy-only case (74.7 vs 74.1).

Table 3: **Effect of Consistency.** Validation accuracy for JS, GJS w/o the consistency term in Proposition 2, and GJS for 40% noise on the CIFAR-100 dataset. Using the mean of two predictions in the JS loss does not improve performance. On the other hand, adding the consistency term significantly helps.

Method	Accuracy
$\mathcal{L}_{JS}(e^{(y)}, \mathbf{p}^{(2)})$	71.0
$\mathcal{L}_{JS_{\pi'}}(e^{(y)}, \mathbf{m}_{>1})$	68.7
$\mathcal{L}_{GJS}(e^{(y)}, \mathbf{p}^{(2)}, \mathbf{p}^{(3)})$	74.3

Table 4: **Effect of GJS.** Validation accuracy when using different loss functions for clean and noisy examples of the CIFAR-100 training set with 40% symmetric noise. Noisy examples benefit significantly more from GJS than clean examples (74.1 vs 72.9).

Method	$\pi_1$				
	Clean	Noisy	0.1	0.5	0.9
JS	JS	70.0	<b>71.5</b>	55.3	
GJS	JS	72.6	<b>72.9</b>	70.2	
JS	GJS	71.0	<b>74.1</b>	68.0	
GJS	GJS	71.3	<b>74.7</b>	73.8	

Table 5: **Effect of Augmentation Strategy.** Validation accuracy for training w/o CutOut(-CO) or w/o RandAug(-RA) or w/o both(weak) on 40% symmetric and asymmetric noise on CIFAR-100. All methods improves by stronger augmentations. GJS performs best for all types of augmentations.

Method	Symmetric				Asymmetric			
	Full	-CO	-RA	Weak	Full	-CO	-RA	Weak
GCE	70.8	64.2	64.1	58.0	51.7	44.9	46.6	42.9
NCE+RCE	68.5	66.6	68.3	61.7	57.5	52.1	49.5	44.4
GJS	<b>74.8</b>	<b>71.3</b>	<b>70.6</b>	<b>66.5</b>	<b>62.6</b>	<b>56.8</b>	<b>52.2</b>	<b>44.9</b>

Table 6: **Effect of Number of Epochs.** Validation accuracy for training with 200 and 400 epochs for 40% symmetric and asymmetric noise on CIFAR-100. GJS still outperforms the baselines and NCE+RCE’s performance is reduced heavily by the decrease in epochs.

Method	Symmetric		Asymmetric	
	200	400	200	400
GCE	70.3	70.8	39.1	51.7
NCE+RCE	60.0	68.5	35.0	57.5
GJS	<b>72.9</b>	<b>74.8</b>	<b>43.2</b>	<b>62.6</b>

**How is different choices of perturbations affecting GJS?** In this work, we use stochastic augmentations for  $\mathcal{A}$ , see Appendix A.1 for details. Table 5 reports validation results on 40% symmetric and asymmetric noise on CIFAR-100 for varying types of augmentation. We observe that all methods improve their performance with stronger augmentation and that GJS achieves the best results in all cases. Also, note that we use weak augmentation for WebVision and still get state-of-the-art results.

**How fast is the convergence?** We found that some baselines (especially the robust NCE+RCE) had slow convergence. Therefore, we used 400 epochs for all methods to make sure all had time to converge properly. Table 6 shows results on 40% symmetric and asymmetric noise on CIFAR-100 when the number of epochs have been reduced by half.

**Summary of experiments in the appendix.** Due to space limitations, we have two important experiments in the appendix. We investigate the importance of 1) losses being symmetric and bounded for learning with noisy labels (Section B.1), and 2) a clean vs noisy validation set for hyperparameter selection and the effect of a single set of parameters for all noise rates (Section B.2).

## 5 Final Remarks

We first made two central observations that (i) robust loss functions have an underfitting issue and (ii) consistency of noise-fitting networks is significantly lower around noisy data points. Correspondingly, we proposed two loss functions, GJS and JS, based on Jensen-Shannon divergence that (i) interpolate between noise-robust MAE and fast-converging CE, and (ii) encourage consistency around training data points. This simple proposal led to state-of-the-art performance on both synthetic and real-world noise datasets even when compared to the more elaborate pipelines such as DivideMix or ELR+. Furthermore, we discussed their robustness within the theoretical construction of Ghosh *et al.* [2]. By drawing further connections to other seminal loss functions such as CE, MAE, GCE, consistency regularization and label smoothing, we uncovered other desirable or informative properties. We further empirically studied different aspects of the losses that corroborated various theoretical properties.

There is still room for a theoretical analysis of the consistency term. This is, in general, an important but understudied area, also for the literature of self or semi-supervised learning and thus is of utmost importance for future works. Furthermore, the proposed loss functions can be studied from an information-theory angle. We find this an important view beyond the scope of this work. A slight practical limitation is the added computations for GJS forward pass *at training time*. However, in all our experiments, we only use one extra prediction ( $M = 3$ ).

Considerable resources are needed to create labelled data sets due to the manual labelling process. Thus, creators of datasets are mostly limited to companies and academic institutions. Developing robust methods against label noise democratizes labelled datasets since imperfect but automatic labelling can be used instead. This gives more people the power to create labelled datasets. On the other hand, it can increase privacy issues arising from exploitation and redistribution of such datasets.

Overall, we believe the paper provides informative theoretical and empirical evidence for the usefulness of two simple and novel JS divergence-based loss functions for learning under noisy data that achieve state-of-the-art results. At the same time it opens interesting future directions.

**Acknowledgement.** This work was partially supported by the Wallenberg AI, Autonomous Systems and Software Program (WASP) funded by the Knut and Alice Wallenberg Foundation.

## References

- [1] Lucas Beyer, Olivier J Hénaff, Alexander Kolesnikov, Xiaohua Zhai, and Aäron van den Oord. Are we done with imagenet? *arXiv preprint arXiv:2006.07159*, 2020.
- [2] Aritra Ghosh, Himanshu Kumar, and PS Sastry. Robust loss functions under label noise for deep neural networks. In *Proceedings of the Thirty-First AAAI Conference on Artificial Intelligence*, pages 1919–1925, 2017.
- [3] Zhilu Zhang and Mert Sabuncu. Generalized cross entropy loss for training deep neural networks with noisy labels. In *Advances in neural information processing systems*, pages 8778–8788, 2018.
- [4] Yisen Wang, Xingjun Ma, Zaiyi Chen, Yuan Luo, Jinfeng Yi, and James Bailey. Symmetric cross entropy for robust learning with noisy labels. In *Proceedings of the IEEE International Conference on Computer Vision*, pages 322–330, 2019.
- [5] Xingjun Ma, Hanxun Huang, Yisen Wang, Simone Romano, Sarah Erfani, and James Bailey. Normalized loss functions for deep learning with noisy labels, 2020.
- [6] Dan Hendrycks, Norman Mu, Ekin D. Cubuk, Barret Zoph, Justin Gilmer, and Balaji Lakshminarayanan. Augmix: A simple data processing method to improve robustness and uncertainty. In *International Conference on Learning Representation*, 2020.
- [7] Avital Oliver, Augustus Odena, Colin Raffel, Ekin D Cubuk, and Ian J Goodfellow. Realistic evaluation of deep semi-supervised learning algorithms. *arXiv preprint arXiv:1804.09170*, 2018.
- [8] Chiyuan Zhang, Samy Bengio, Moritz Hardt, Benjamin Recht, and Oriol Vinyals. Understanding deep learning requires rethinking generalization, 2017.
- [9] Yang Liu and Hongyi Guo. Peer loss functions: Learning from noisy labels without knowing noise rates. In Hal Daumé III and Aarti Singh, editors, *Proceedings of the 37th International Conference on Machine Learning*, volume 119 of *Proceedings of Machine Learning Research*, pages 6226–6236. PMLR, 13–18 Jul 2020.
- [10] Nagarajan Natarajan, Inderjit S Dhillon, Pradeep K Ravikumar, and Ambuj Tewari. Learning with noisy labels. In *Advances in neural information processing systems*, pages 1196–1204, 2013.
- [11] Sainbayar Sukhbaatar, Joan Bruna, Manohar Paluri, Lubomir Bourdev, and Rob Fergus. Training convolutional networks with noisy labels. In *Proceedings of the international conference on learning representation*, 2015.
- [12] Giorgio Patrini, Alessandro Rozza, Aditya Krishna Menon, Richard Nock, and Lizhen Qu. Making deep neural networks robust to label noise: A loss correction approach. In *Proceedings of the IEEE Conference on Computer Vision and Pattern Recognition*, pages 1944–1952, 2017.
- [13] Bo Han, Jiangchao Yao, Gang Niu, Mingyuan Zhou, Ivor Tsang, Ya Zhang, and Masashi Sugiyama. Masking: A new perspective of noisy supervision. In *Advances in Neural Information Processing Systems*, pages 5836–5846, 2018.
- [14] Xiaobo Xia, Tongliang Liu, Nannan Wang, Bo Han, Chen Gong, Gang Niu, and Masashi Sugiyama. Are anchor points really indispensable in label-noise learning? In *Advances in Neural Information Processing Systems*, pages 6838–6849, 2019.
- [15] Junnan Li, Richard Socher, and Steven CH Hoi. Dividemix: Learning with noisy labels as semi-supervised learning. In *International Conference on Learning Representation*, 2020.
- [16] Yilun Xu, Peng Cao, Yuqing Kong, and Yizhou Wang. L\_dmi: A novel information-theoretic loss function for training deep nets robust to label noise. In *Advances in Neural Information Processing Systems*, pages 6225–6236, 2019.
- [17] Jiaheng Wei and Yang Liu. When optimizing f-divergence is robust with label noise. In *International Conference on Learning Representation*, 2021.
- [18] Giorgio Patrini, Alessandro Rozza, Aditya Menon, Richard Nock, and Lizhen Qu. Making deep neural networks robust to label noise: a loss correction approach, 2017.
- [19] Michal Lukasik, Srinadh Bhojanapalli, Aditya Krishna Menon, and Sanjiv Kumar. Does label smoothing mitigate label noise? In *International Conference on Machine Learning*, 2020.

- [20] Scott Reed, Honglak Lee, Dragomir Anguelov, Christian Szegedy, Dumitru Erhan, and Andrew Rabinovich. Training deep neural networks on noisy labels with bootstrapping. *arXiv preprint arXiv:1412.6596*, 2014.
- [21] Evgenii Zheltonozhskii, Chaim Baskin, Avi Mendelson, Alex M. Bronstein, and Or Litany. Contrast to divide: Self-supervised pre-training for learning with noisy labels, 2021.
- [22] Sheng Liu, Jonathan Niles-Weed, Narges Razavian, and Carlos Fernandez-Granda. Early-learning regularization prevents memorization of noisy labels, 2020.
- [23] Wen Li, Limin Wang, Wei Li, Eirikur Agustsson, and Luc Van Gool. Webvision database: Visual learning and understanding from web data, 2017.
- [24] Lu Jiang, Zhenyuan Zhou, Thomas Leung, Jia Li, and Fei-Fei Li. Mentornet: Learning data-driven curriculum for very deep neural networks on corrupted labels. In *ICML*, 2018.
- [25] Ekin D. Cubuk, Barret Zoph, Jonathon Shlens, and Quoc V. Le. Randaugment: Practical automated data augmentation with a reduced search space, 2019.
- [26] Terrance DeVries and Graham W. Taylor. Improved regularization of convolutional neural networks with cutout, 2017.
- [27] Junnan Li, Yongkang Wong, Qi Zhao, and Mohan Kankanhalli. Learning to learn from noisy labeled data, 2019.
- [28] Jianhua Lin. Divergence measures based on the shannon entropy. *IEEE Transactions on Information theory*, 37(1):145–151, 1991.
- [29] Duc Tam Nguyen, Chaithanya Kumar Mummadli, Thi Phuong Nhung Ngo, Thi Hoai Phuong Nguyen, Laura Beggel, and Thomas Brox. Self: Learning to filter noisy labels with self-ensembling. In *International Conference on Learning Representation*, 2019.
- [30] Curtis G Northcutt, Tailin Wu, and Isaac L Chuang. Learning with confident examples: Rank pruning for robust classification with noisy labels. *arXiv preprint arXiv:1705.01936*, 2017.
- [31] Daiki Tanaka, Daiki Ikami, Toshihiko Yamasaki, and Kiyoharu Aizawa. Joint optimization framework for learning with noisy labels. In *Proceedings of the IEEE Conference on Computer Vision and Pattern Recognition*, pages 5552–5560, 2018.
- [32] Arash Vahdat. Toward robustness against label noise in training deep discriminative neural networks. In *Advances in Neural Information Processing Systems*, pages 5596–5605, 2017.
- [33] Ahmet Iscen, Giorgos Tolias, Yannis Avrithis, Ondrej Chum, and Cordelia Schmid. Graph convolutional networks for learning with few clean and many noisy labels. In *Proceedings of the European Conference on Computer Vision*, 2020.
- [34] Paul Hongsuck Seo, Geeho Kim, and Bohyung Han. Combinatorial inference against label noise. In *Advances in Neural Information Processing Systems*, pages 1173–1183, 2019.
- [35] Christian Szegedy, Vincent Vanhoucke, Sergey Ioffe, Jon Shlens, and Zbigniew Wojna. Rethinking the inception architecture for computer vision. In *Proceedings of the IEEE conference on computer vision and pattern recognition*, pages 2818–2826, 2016.
- [36] Takeru Miyato, Shin-ichi Maeda, Masanori Koyama, and Shin Ishii. Virtual adversarial training: a regularization method for supervised and semi-supervised learning. *IEEE transactions on pattern analysis and machine intelligence*, 41(8):1979–1993, 2018.
- [37] David Berthelot, Nicholas Carlini, Ian Goodfellow, Nicolas Papernot, Avital Oliver, and Colin A Raffel. Mixmatch: A holistic approach to semi-supervised learning. In *Advances in Neural Information Processing Systems*, pages 5049–5059, 2019.
- [38] Antti Tarvainen and Harri Valpola. Mean teachers are better role models: Weight-averaged consistency targets improve semi-supervised deep learning results. In *Advances in neural information processing systems*, pages 1195–1204, 2017.

## A Training Details

All proposed losses and baselines use the same training settings, which are described in detail here.

### A.1 CIFAR

**General training details.** For all the results on the CIFAR datasets, we use a PreActResNet-34 with a standard SGD optimizer with Nesterov momentum, and a batch size of 128. For the network, we use three stacks of five residual blocks with 32, 64, and 128 filters for the layers in these stacks, respectively. The learning rate is reduced by a factor of 10 at 50% and 75% of the total 400 epochs. For data augmentation, we use RandAugment [25] with  $N = 1$  and  $M = 3$  using random cropping (size 32 with 4 pixels as padding), random horizontal flipping, normalization and lastly Cutout [26] with length 16. We set random seeds for all methods to have the same network weight initialization, order of data for the data loader, train-validation split, and noisy labels in the training set. We use a clean validation set corresponding to 10% of the training data. A clean validation set is commonly provided with real-world noisy datasets [23, 27]. Any potential gain from using a clean instead of a noisy validation set is the same for all methods since all share the same setup.

**JS and GJS implementation.** We implement the Jensen-Shannon-based losses using the definitions based on KL divergence, see Equation 2. To make sure the gradients are propagated through the target argument, we do not use the KL divergence in PyTorch. Instead, we write our own based on the official implementation.

**Search for learning rate and weight decay.** We do a separate hyperparameter search for learning rate and weight decay on 40% noise using both asymmetric and symmetric noises on CIFAR datasets. For CIFAR-10, we search for learning rates in  $[0.001, 0.005, 0.01, 0.05, 0.1]$  and weight decays in  $[1e-4, 5e-4, 1e-3]$ . The method-specific hyperparameters used for this search were 0.9, 0.7, (0.1, 1.0), 0.7, (1.0, 1.0), 0.5, 0.5 for  $BS(\beta)$ ,  $LS(\epsilon)$ ,  $SCE(\alpha, \beta)$ ,  $GCE(q)$ ,  $NCE+RCE(\alpha, \beta)$ ,  $JS(\pi_1)$  and  $GJS(\pi_1)$ , respectively. For CIFAR-100, we search for learning rates in  $[0.01, 0.05, 0.1, 0.2, 0.4]$  and weight decays in  $[1e-5, 5e-5, 1e-4]$ . The method-specific hyperparameters used for this search were 0.9, 0.7, (6.0, 0.1), 0.7, (10.0, 0.1), 0.5, 0.5 for  $BS(\beta)$ ,  $LS(\epsilon)$ ,  $SCE(\alpha, \beta)$ ,  $GCE(q)$ ,  $NCE+RCE(\alpha, \beta)$ ,  $JS(\pi_1)$  and  $GJS(\pi_1)$ , respectively. Note that, these fixed method-specific hyperparameters for both CIFAR-10 and CIFAR-100 are taken from their corresponding papers for this initial search of learning rate and weight decay but they will be further optimized systematically in the next steps.

**Search for method-specific parameters.** We fix the obtained best learning rate and weight decay for all other noise rates, but then for each noise rate/type, we search for method-specific parameters. For the methods with a single hyperparameter,  $BS(\beta)$ ,  $LS(\epsilon)$ ,  $GCE(q)$ ,  $JS(\pi_1)$ ,  $GJS(\pi_1)$ , we try values in  $[0.1, 0.3, 0.5, 0.7, 0.9]$ . On the other hand,  $NCE+RCE$  and  $SCE$  have three hyperparameters, *i.e.*  $\alpha$  and  $\beta$  that scale the two loss terms, and  $A := \log(0)$  for the RCE term. We set  $A = \log(1e-4)$  and do a grid search for three values of  $\alpha$  and two of beta  $\beta$  (six in total) around the best reported parameters from each paper.<sup>2</sup>

**Test evaluation.** The best parameters are then used to train on the full training set with five different seeds. The final parameters that were used to get the results in Table 1 are shown in Table 7.

For completeness, in Appendix B.2, we provide results for a less thorough hyperparameter search (more similar to related work) which also use a noisy validation set.

### A.2 WebVision

All methods train a randomly initialized ResNet-50 model from PyTorch using the SGD optimizer with Nesterov momentum, and a batch size of 32 for GJS and 64 for CE and JS. For data augmentation, we do a random resize crop of size 224, random horizontal flips, and color jitter (torchvision ColorJitter transform with brightness=0.4, contrast=0.4, saturation=0.4, hue=0.2). We use a fixed weight decay of  $1e-4$  and do a grid search for the best learning rate in  $[0.1, 0.2, 0.4]$  and  $\pi_1 \in [0.1, 0.3, 0.5, 0.7, 0.9]$ . The learning rate is reduced by a multiplicative factor of 0.97 every epoch, and we train for a total of 300 epochs. The best starting learning rates were 0.4, 0.2, 0.1 for CE, JS and GJS, respectively.

<sup>2</sup>We also tried using  $\beta = 1 - \alpha$ , and mapping the best parameters from the papers to this range, combined with a similar search as for the single parameter methods, but this resulted in worse performance.

Table 7: **Hyperparameters for CIFAR.** A hyperparameter search over learning rates and weight decays, was done for 40% noise on both symmetric and asymmetric noise for the CIFAR datasets. The best parameters for each method are shown in this table, where the format is [learning rate, weight decay]. The hyperparameters for zero percent noise uses the same settings as for the symmetric noise. For the best learning rate and weight decay, another search is done for method-specific hyperparameters, and the best values are shown here. For methods with a single hyperparameter, the value correspond to their respective hyperparameter, i.e., BS ( $\beta$ ), LS ( $\epsilon$ ), GCE ( $q$ ), JS ( $\pi_1$ ), GJS ( $\pi_1$ ). For NCE+RCE and SCE the value correspond to  $[\alpha, \beta]$ .

Dataset	Method	Learning Rate & Weight Decay				Method-specific Hyperparameters							
		Sym Noise		Asym Noise		No Noise		Sym Noise				Asym Noise	
		20-80%	20-40%	0%	20%	40%	60%	80%	20%	40%	20%	40%	
CIFAR-10	CE	[0.05, 1e-3]	[0.1, 1e-3]	-	-	-	-	-	-	-	-	-	
	BS	[0.1, 1e-3]	[0.1, 1e-3]	0.5	0.5	0.7	0.7	0.9	0.7	0.5	0.7	0.5	
	LS	[0.1, 5e-4]	[0.1, 1e-3]	0.1	0.5	0.9	0.7	0.1	0.1	0.1	0.1	0.1	
	SCE	[0.01, 5e-4]	[0.05, 1e-3]	[0.2, 0.1]	[0.05, 0.1]	[0.1, 0.1]	[0.2, 1.0]	[0.1, 1.0]	[0.1, 0.1]	[0.2, 1.0]	[0.1, 0.1]	[0.2, 1.0]	
	GCE	[0.01, 5e-4]	[0.1, 1e-3]	0.5	0.7	0.7	0.7	0.9	0.1	0.1	0.1	0.1	
	NCE+RCE	[0.005, 1e-3]	[0.05, 1e-4]	[10, 0.1]	[10, 0.1]	[10, 0.1]	[10, 0.1]	[10, 1.0]	[10, 0.1]	[10, 0.1]	[10, 0.1]	[10, 0.1]	
	JS	[0.01, 5e-4]	[0.1, 1e-3]	0.1	0.7	0.7	0.9	0.9	0.3	0.3	0.3	0.3	
CIFAR-100	GJS	[0.1, 5e-4]	[0.1, 1e-3]	0.5	0.3	0.9	0.1	0.1	0.3	0.3	0.3	0.3	
	CE	[0.4, 1e-4]	[0.2, 1e-4]	-	-	-	-	-	-	-	-	-	
	BS	[0.4, 1e-4]	[0.4, 1e-4]	0.7	0.5	0.5	0.5	0.9	0.3	0.3	0.3	0.3	
	LS	[0.2, 5e-5]	[0.4, 1e-4]	0.1	0.7	0.7	0.7	0.9	0.5	0.7	0.5	0.7	
	SCE	[0.2, 1e-4]	[0.4, 5e-5]	[0.1, 0.1]	[0.1, 0.1]	[0.1, 0.1]	[0.1, 1.0]	[0.1, 0.1]	[0.1, 1.0]	[0.1, 1.0]	[0.1, 1.0]	[0.1, 1.0]	
	GCE	[0.4, 1e-5]	[0.2, 1e-4]	0.5	0.5	0.5	0.7	0.7	0.7	0.7	0.7	0.7	
	NCE+RCE	[0.2, 5e-5]	[0.2, 5e-5]	[20, 0.1]	[20, 0.1]	[20, 0.1]	[20, 0.1]	[20, 0.1]	[20, 0.1]	[20, 0.1]	[20, 0.1]	[10, 0.1]	
CIFAR-100	JS	[0.2, 1e-4]	[0.1, 1e-4]	0.1	0.1	0.3	0.5	0.3	0.5	0.5	0.5	0.5	
	GJS	[0.2, 5e-5]	[0.4, 1e-4]	0.3	0.3	0.5	0.9	0.1	0.5	0.5	0.5	0.1	

Both JS and GJS used  $\pi_1 = 0.1$ . With the best learning rate and  $\pi_1$ , we ran four more runs with new seeds for the network initialization and data loader.

### A.3 Computational Resources

For all our experiments, we use an internal cluster of NVIDIA GeForce RTX 2080 Ti graphics cards. We estimate the total amount of compute (including hyperparameter searches) to be at least 524 GPU days ( $\sim 357$  for Table 1,  $\sim 77$  for Table 2, and  $\sim 90$  for Table 9).

## B Additional Insights and Experiments

### B.1 Towards a better understanding of JS

In Proposition 2, we showed that JS is an important part of GJS, and therefore deserves attention. Here, we make a systematic *ablation study* to empirically examine the contribution of the difference(s) between JS loss and CE. We decompose the JS loss following the gradual construction of the Jensen-Shannon divergence in the work of Lin *et al.* [28]. This construction, interestingly, lends significant empirical evidence to bounded losses’ robustness to noise, in connection to Theory 1 and Proposition 3.

Let  $KL(\mathbf{p}, \mathbf{q})$  denote the KL-divergence of a predictive distribution  $\mathbf{q} \in \Delta^{K-1}$  from a target distribution  $\mathbf{p} \in \Delta^{K-1}$ . KL divergence is neither symmetric nor bounded.  $K$  divergence, proposed by Lin *et al.* [28], is a bounded version defined as  $K(\mathbf{p}, \mathbf{q}) := KL(\mathbf{p}, (\mathbf{p} + \mathbf{q})/2) = KL(\mathbf{p}, \mathbf{m})$ . However, this divergence is not symmetric. A simple way to achieve symmetry is to take the average of forward and reverse versions of a divergence. For  $KL$  and  $K$ , this gives rise to Jeffrey’s divergence and JS with  $\pi = [\frac{1}{2}, \frac{1}{2}]^T$ , respectively. Table 8 provides an overview of these divergences and Figure 6 shows their validation accuracy during training on CIFAR-100 with 40% symmetric noise.

Table 8: **Ablation Study of JS.** A comparison of JS and other KL-based divergences and their relationship to symmetry and boundedness. The distribution  $\mathbf{m}$  is the mean of  $\mathbf{p}$  and  $\mathbf{q}$ .

Method	Formula	Symmetric	Bounded
KL	$KL(\mathbf{p}, \mathbf{q})$		
KL'	$KL(\mathbf{q}, \mathbf{p})$		
Jeffrey's	$(KL(\mathbf{p}, \mathbf{q}) + KL(\mathbf{q}, \mathbf{p}))/2$	✓	
K	$KL(\mathbf{p}, \mathbf{m})$		✓
K'	$KL(\mathbf{q}, \mathbf{m})$		✓
JS	$(KL(\mathbf{p}, \mathbf{m}) + KL(\mathbf{q}, \mathbf{m}))/2$	✓	✓

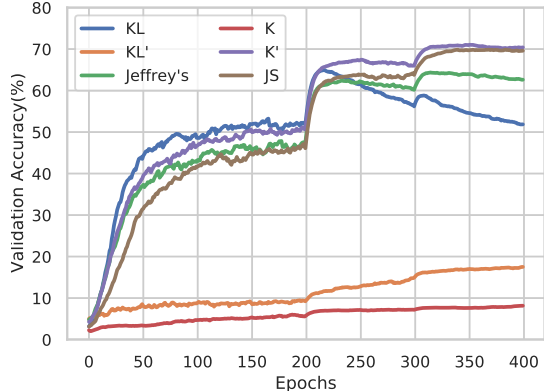


Figure 6: **Ablation Study of JS.** Validation accuracy of the divergences in Table 8 are plotted during training with 40% symmetric noise on the CIFAR-100 dataset. Notably, the only two losses that show signs of overfitting ( $KL$  and Jeffrey's) are unbounded. Interestingly,  $K$  (bounded  $KL$ ) makes the learning slower, while  $K'$  (bounded  $KL'$ ) considerably improves the learning dynamics. Finally, it can be seen that, JS, in contrast to its unbounded version (Jeffrey's), does not overfit to noise.

**Bounded.** Notably, the only two losses that show signs of overfitting ( $KL$  and Jeffrey's) are unbounded. Interestingly,  $K$  (bounded  $KL$ ) makes the learning much slower, while  $K'$  (bounded  $KL'$ ) considerably improves the learning dynamics. Finally, it can be seen that, JS, in contrast to its unbounded version (Jeffrey's), does not overfit to noise.

**Symmetry.** The Jeffrey's divergence performs better than either of its two constituent  $KL$  terms. This is not as clear for JS, where  $K'$  is performing surprisingly well on its own. In the proof of Proposition 1, we show that  $K' \rightarrow \text{MAE}$  as  $\pi_1 \rightarrow 1$ , while  $K$  goes to zero, which could explain why  $K'$  seems to be robust to noise. Furthermore,  $K'$ , which is a component of JS, is reminiscent of label smoothing.

Beside the bound and symmetry, other notable properties of JS and GJS are the connections to MAE and consistency losses. Next section investigates the effect of hyperparameters that substantiates the connection to MAE (Proposition 1).

## B.2 Noisy Validation Set & Single Set of Parameters

Our systematic procedure to search for hyperparameters (A.1) is done to have a more conclusive comparison to other methods. The most common procedure in related works is for each dataset, all methods use the same learning rate and weight decay(chosen seemingly arbitrary), and each method uses a single set of method-specific parameters for all noise rates and types. Baselines typically use the same method-specific parameters as reported in their respective papers. First, using the same learning rate and weight decay is problematic when comparing loss functions that have different gradient magnitudes. Second, directly using the parameters reported for the baselines is also problematic since the optimal hyperparameters depend on the training setup, which could be different, e.g., network architecture, augmentation, learning rate schedule, etc. Third, using a fixed method-specific parameter for all noise rates makes the results highly dependent on this choice. Lastly, it is not possible to know if other methods would have performed better if a proper hyperparameter search was done.

Here, for completeness, we use the same setup as in Section A.1, except we use the same learning rate and weight decay for all methods and search for hyperparameters based on a noisy validation set (more similar to related work).

Table 9: **Synthetic Noise Benchmark on CIFAR**. We reimplement other noise-robust loss functions into the *same learning setup* and ResNet-34, including label smoothing (LS), Bootstrap (BS), Symmetric CE (SCE), Generalized CE (GCE), and Normalized CE (NCE+RCE). We used *same hyperparameter optimization budget and mechanism* for all the prior works and ours. All methods use the same learning rate and weight decay and use the optimal method-specific parameters from a search on 40% symmetric noise based on noisy validation accuracy. Mean test accuracy and standard deviation are reported from five runs and the statistically-significant top performers are boldfaced.

Dataset	Method	No Noise		Symmetric Noise Rate				Asymmetric Noise Rate	
		0%	20%	40%	60%	80%	20%	40%	
CIFAR-10	CE	<b>95.66 ± 0.18</b>	91.47 ± 0.28	87.31 ± 0.29	81.96 ± 0.38	65.28 ± 0.90	92.80 ± 0.64	85.82 ± 0.42	
	BS	95.47 ± 0.11	93.65 ± 0.23	90.77 ± 0.30	49.80 ± 20.64	32.91 ± 5.43	93.86 ± 0.14	85.37 ± 1.07	
	LS	95.45 ± 0.15	93.52 ± 0.09	89.94 ± 0.17	84.13 ± 0.80	62.76 ± 2.00	92.71 ± 0.41	83.61 ± 1.21	
	SCE	94.92 ± 0.18	93.41 ± 0.20	90.99 ± 0.20	86.04 ± 0.31	41.04 ± 4.56	93.26 ± 0.13	84.46 ± 1.22	
	GCE	94.94 ± 0.09	93.79 ± 0.19	91.45 ± 0.17	86.00 ± 0.20	62.01 ± 2.54	93.23 ± 0.12	85.92 ± 0.61	
	NCE+RCE	94.31 ± 0.16	92.79 ± 0.16	90.31 ± 0.23	84.80 ± 0.47	34.47 ± 14.66	92.99 ± 0.15	87.00 ± 1.05	
	JS	94.74 ± 0.21	93.53 ± 0.23	91.57 ± 0.22	86.21 ± 0.48	65.87 ± 2.92	92.97 ± 0.26	86.42 ± 0.36	
	GJS	<b>95.86 ± 0.10</b>	<b>95.20 ± 0.11</b>	<b>94.13 ± 0.19</b>	<b>89.65 ± 0.26</b>	<b>76.74 ± 0.75</b>	<b>94.81 ± 0.10</b>	<b>90.29 ± 0.26</b>	
CIFAR-100	CE	77.84 ± 0.17	65.74 ± 0.06	55.57 ± 0.55	44.60 ± 0.79	10.74 ± 5.11	66.61 ± 0.45	50.42 ± 0.44	
	BS	77.63 ± 0.25	73.01 ± 0.28	68.35 ± 0.43	54.07 ± 1.16	2.43 ± 0.49	69.75 ± 0.35	50.61 ± 0.32	
	LS	77.60 ± 0.28	74.22 ± 0.30	66.84 ± 0.28	54.09 ± 0.71	21.00 ± 2.14	73.30 ± 0.42	<b>57.02 ± 0.57</b>	
	SCE	77.46 ± 0.39	73.26 ± 0.29	66.96 ± 0.27	54.09 ± 0.49	13.26 ± 2.31	71.22 ± 0.33	49.91 ± 0.28	
	GCE	76.70 ± 0.39	74.14 ± 0.32	70.41 ± 0.40	62.14 ± 0.27	12.38 ± 3.74	69.40 ± 0.30	48.54 ± 0.30	
	NCE+RCE	73.23 ± 0.34	70.19 ± 0.27	65.61 ± 0.87	50.33 ± 1.58	5.55 ± 1.67	69.47 ± 0.25	56.32 ± 0.33	
	JS	77.20 ± 0.53	74.47 ± 0.25	70.12 ± 0.39	61.69 ± 0.63	<b>27.77 ± 4.11</b>	67.21 ± 0.37	49.39 ± 0.13	
	GJS	<b>78.76 ± 0.32</b>	<b>77.14 ± 0.45</b>	<b>74.69 ± 0.12</b>	<b>64.06 ± 0.52</b>	12.95 ± 2.40	<b>74.44 ± 0.49</b>	52.34 ± 0.81	

The learning rate and weight decay for all methods are chosen based on noisy validation accuracy for CE on 40% symmetric noise for each dataset. The optimal learning rates and weight decays([lr,wd]) were [0.05, 1e-3] and [0.4, 1e-4] for CIFAR-10 and CIFAR-100, respectively. The method-specific parameters are found by a similar search as in Section A.1, except it is only done for 40% symmetric noise and the optimal parameters are used for all other noise rates and types. For CIFAR-10, the optimal method-specific hyperparameters were 0.5, 0.5, (0.1, 0.1), 0.5, (10, 0.1), 0.5, 0.3 for BS( $\beta$ ), LS( $\epsilon$ ), SCE( $\alpha, \beta$ ), GCE( $q$ ), NCE+RCE( $\alpha, \beta$ ), JS( $\pi_1$ ) and GJS( $\pi_1$ ), respectively. For CIFAR-100, the optimal method-specific hyperparameters were 0.5, 0.7, (0.1, 0.1), 0.5, (20, 0.1), 0.1, 0.5 for BS( $\beta$ ), LS( $\epsilon$ ), SCE( $\alpha, \beta$ ), GCE( $q$ ), NCE+RCE( $\alpha, \beta$ ), JS( $\pi_1$ ) and GJS( $\pi_1$ ), respectively. The results with this setup can be seen in Table 9.

### B.3 Comparison between JS and GCE

We were pleasantly surprised by the finding in Proposition 1 that JS generalizes CE and MAE, similarly to GCE. Here, we highlight differences between JS and GCE.

**Theoretical properties.** Our inspiration to study JS came from the *symmetric* loss function of SCE, and the *bounded* loss of GCE. JS has *both* properties and a rich history in the field of information theory. This is also one of the reasons we studied these properties in Section B.1. Finally, JS generalizes naturally to more than two distributions.

**Gradients.** The gradients of CE/KL, GCE, JS and MAE with respect to logit  $z_i$  of prediction  $\mathbf{p} = [p_1, p_2, \dots, p_K]$ , given a label  $e^{(y)}$ , are of the form  $-\frac{\partial p_y}{\partial z_i} g(p_y)$  with  $g(p_y)$  being  $\frac{1}{p_y}$ ,  $\frac{1}{p_y^{1-q}}$ ,  $(1 - \pi_1) \log \left( \frac{\pi_1}{(1 - \pi_1)p_y} + 1 \right) / Z$ , and 1, for each of these losses respectively. Note that,  $q$  is the hyperparameter of GCE and  $p_y$  denotes the  $y$ th component of  $\mathbf{p}$ .

In Figure 7, these gradients are compared by varying the hyperparameter of GCE,  $q \in [0.1, 0.3, 0.5, 0.7, 0.9]$ , and finding the corresponding  $\pi$  for  $JS_\pi$  such that the two gradients are equal at  $p_y = \frac{1}{2}$ .

Looking at the behaviour of the different losses at low- $p_y$  regime, intuitively, a high gradient scale for low  $p_y$  means a large parameter update for deviating from the given class. This can make noise free learning faster by pushing the probability to the correct class, which is what CE does. However, if the

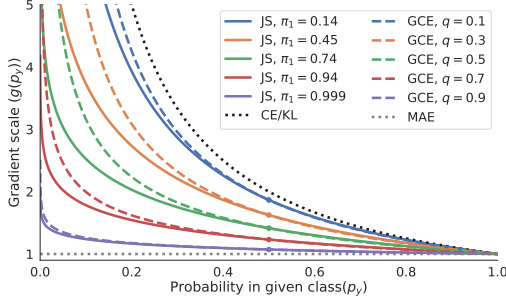


Figure 7: **Comparison between JS and GCE.** A comparison of gradients scales between JS and GCE. For each  $q$  of GCE, a corresponding  $\pi_1$  of JS is chosen such that the gradient scales are equal at  $p_y = \frac{1}{2}$ .

given class is incorrect (noisy) this can cause overfitting. The gradient scale of MAE induces same update magnitude for  $p_y$ , which can give the network more freedom to deviate from noisy classes, at the cost of slower learning for the correctly labeled examples.

Comparing GCE and  $JS_{\pi}$  in Figure 7, it can be seen that  $JS_{\pi}$  generally penalize lower probability in the given class less than what GCE does. In this sense,  $JS_{\pi}$  behaves more like MAE.

For a derivation of the gradients of  $D_{JS}$ , see Section C.6.

**Label distributions.** GCE requires the label distribution to be onehot which makes it harder to incorporate GCE in many of the elaborate state-of-the-art methods that use “soft labels” *e.g.*, Mixup, co-training, or knowledge distillation.

#### B.4 Consistency Measure

In this section, we provide more details about the consistency measure used in Figure 1. To be independent of any particular loss function, we considered a measure similar to standard Top-1 accuracy. We measure the ratio of samples that predict the same class on both the original image and an augmented version of it

$$\frac{1}{N} \sum_{i=1}^N \mathbb{1} \left( \arg \max_y f(\mathbf{x}_i) = \arg \max_y f(\tilde{\mathbf{x}}_i) \right) \quad (7)$$

where the sum is over all the training examples, and  $\mathbb{1}$  is the indicator function, the argmax is over the predicted probability of  $K$  classes, and  $\tilde{\mathbf{x}}_i \sim \mathcal{A}(\mathbf{x}_i)$  is an augmented version of  $\mathbf{x}_i$ . Notably, this measure does not depend on the labels.

In the experiment in Figure 1, the original images are only normalized, while the augmented images use the same augmentation strategy as the benchmark experiments, see Section A.1.

## C Proofs

### C.1 Noise Robustness

The proofs of the theorems in this sections are generalizations of the proofs in by Zhang *et al.* [3]. The original theorems are specific to their particular GCE loss and cannot directly be used for other loss functions. We generalize the theorems to be useful for any loss function satisfying certain conditions(bounded and conditions in Lemma 1). To be able to use the theorems for GJS, we also generalize them to work for more than a single predictive distribution. Here, we use  $(\mathbf{x}, y)$  to denote a sample from  $\mathcal{D}$  and  $(\mathbf{x}, \hat{y})$  to denote a sample from  $\mathcal{D}_{\eta}$ . Let  $\eta_{ij}$  denote the probability that a sample of class  $i$  was changed to class  $j$  due to noise.

**Theorem 1.** Under symmetric noise with  $\eta < \frac{K-1}{K}$ , if  $B_L \leq \sum_{i=1}^K \mathcal{L}(\mathbf{e}^{(i)}, \mathbf{x}, f) \leq B_U, \forall \mathbf{x}, f$  is satisfied for a loss  $\mathcal{L}$ , then

$$0 \leq R_{\mathcal{L}}^{\eta}(f^*) - R_{\mathcal{L}}^{\eta}(f_{\eta}) \leq \eta \frac{B_U - B_L}{K-1}, \quad \text{and} \quad -\frac{\eta(B_U - B_L)}{K-1 - \eta K} \leq R_{\mathcal{L}}(f^*) - R_{\mathcal{L}}(f_{\eta}) \leq 0, \quad (5)$$

*Proof of Theorem 1.* For any function,  $f$ , mapping an input  $\mathbf{x} \in \mathbb{X}$  to  $\Delta^{K-1}$ , we have

$$R_{\mathcal{L}}(f) = \mathbb{E}_{\mathcal{D}}[\mathcal{L}(\mathbf{e}^{(y)}, \mathbf{x}, f)] = \mathbb{E}_{\mathbf{x}, y}[\mathcal{L}(\mathbf{e}^{(y)}, \mathbf{x}, f)]$$

and for uniform noise with noise rate  $\eta$ , the probability of a class not changing label due to noise is  $\eta_{ii} = 1 - \eta$ , while the probability of changing from one class to any other is  $\eta_{ij} = \frac{\eta}{K-1}$ . Therefore,

$$\begin{aligned} R_{\mathcal{L}}^{\eta}(f) &= \mathbb{E}_{\mathcal{D}_{\eta}}[\mathcal{L}(\mathbf{e}^{(\tilde{y})}, \mathbf{x}, f)] = \mathbb{E}_{\mathbf{x}, \tilde{y}}[\mathcal{L}(\mathbf{e}^{(\tilde{y})}, \mathbf{x}, f)] \\ &= \mathbb{E}_{\mathbf{x}} \mathbb{E}_{y|\mathbf{x}} \mathbb{E}_{\tilde{y}|y, \mathbf{x}}[\mathcal{L}(\mathbf{e}^{(\tilde{y})}, \mathbf{x}, f)] \\ &= \mathbb{E}_{\mathbf{x}} \mathbb{E}_{y|\mathbf{x}}[(1 - \eta) \mathcal{L}(\mathbf{e}^{(y)}, \mathbf{x}, f) + \frac{\eta}{K-1} \sum_{i \neq y}^K \mathcal{L}(\mathbf{e}^{(i)}, \mathbf{x}, f)] \\ &= \mathbb{E}_{\mathbf{x}} \mathbb{E}_{y|\mathbf{x}} \left[ (1 - \eta) \mathcal{L}(\mathbf{e}^{(y)}, \mathbf{x}, f) + \frac{\eta}{K-1} \left( \sum_{i=1}^K \mathcal{L}(\mathbf{e}^{(i)}, \mathbf{x}, f) - \mathcal{L}(\mathbf{e}^{(y)}, \mathbf{x}, f) \right) \right] \\ &= \left( 1 - \eta - \frac{\eta}{K-1} \right) R_{\mathcal{L}}(f) + \frac{\eta}{K-1} \mathbb{E}_{\mathbf{x}} \mathbb{E}_{y|\mathbf{x}} \left[ \sum_{i=1}^K \mathcal{L}(\mathbf{e}^{(i)}, \mathbf{x}, f) \right] \\ &= \left( 1 - \frac{\eta K}{K-1} \right) R_{\mathcal{L}}(f) + \frac{\eta}{K-1} \mathbb{E}_{\mathbf{x}} \mathbb{E}_{y|\mathbf{x}} \left[ \sum_{i=1}^K \mathcal{L}(\mathbf{e}^{(i)}, \mathbf{x}, f) \right] \end{aligned}$$

Using the bounds  $B_L \leq \sum_{k=1}^K \mathcal{L}(\mathbf{e}^{(k)}, \mathbf{x}, f) \leq B_U$ , we get:

$$\left( 1 - \frac{\eta K}{K-1} \right) R_{\mathcal{L}}(f) + \frac{\eta B_L}{K-1} \leq R_{\mathcal{L}}^{\eta}(f) \leq \left( 1 - \frac{\eta K}{K-1} \right) R_{\mathcal{L}}(f) + \frac{\eta B_U}{K-1}$$

With these bounds, the difference between  $R_{\mathcal{L}}^{\eta}(f^*)$  and  $R_{\mathcal{L}}^{\eta}(f_{\eta})$  can be bounded as follows

$$\begin{aligned} R_{\mathcal{L}}^{\eta}(f^*) - R_{\mathcal{L}}^{\eta}(f_{\eta}) &\leq \left( 1 - \frac{\eta K}{K-1} \right) R_{\mathcal{L}}(f^*) + \frac{\eta B_U}{K-1} - \left( \left( 1 - \frac{\eta K}{K-1} \right) R_{\mathcal{L}}(f_{\eta}) + \frac{\eta B_L}{K-1} \right) = \\ &= \left( 1 - \frac{\eta K}{K-1} \right) (R_{\mathcal{L}}(f^*) - R_{\mathcal{L}}(f_{\eta})) + \frac{\eta(B_U - B_L)}{K-1} \leq \frac{\eta(B_U - B_L)}{K-1} \end{aligned}$$

where the last inequality follows from the assumption on the noise rate,  $(1 - \frac{\eta K}{K-1}) > 0$ , and that  $f^*$  is the minimizer of  $R_{\mathcal{L}}(f)$  so  $R_{\mathcal{L}}(f^*) - R_{\mathcal{L}}(f_{\eta}) \leq 0$ . Similarly, since  $f_{\eta}^*$  is the minimizer of  $R_{\mathcal{L}}^{\eta}(f)$ , we have  $R_{\mathcal{L}}^{\eta}(f^*) - R_{\mathcal{L}}^{\eta}(f_{\eta}^*) \geq 0$ , which is the lower bound.  $\square$

**Lemma 1.** Consider the following conditions for a loss with label  $\mathbf{e}^{(i)}$ , for any  $i \in \{1, 2, \dots, K\}$  and  $M-1$  distributions  $\mathbf{p}^{(2)}, \dots, \mathbf{p}^{(M)} \in \Delta^{K-1}$ :

- i)  $\mathcal{L}(\mathbf{e}^{(i)}, \mathbf{p}^{(2)}, \dots, \mathbf{p}^{(M)}) = 0 \iff \mathbf{p}^{(2)}, \dots, \mathbf{p}^{(M)} = \mathbf{e}^{(i)}$ ,
- ii)  $0 \leq \mathcal{L}(\mathbf{e}^{(i)}, \mathbf{p}^{(2)}, \dots, \mathbf{p}^{(M)}) \leq C_1$ ,
- iii)  $\mathcal{L}(\mathbf{e}^{(i)}, \mathbf{e}^{(j)}, \dots, \mathbf{e}^{(j)}) = C_2 \leq C_1$ , with  $i \neq j$ .

where  $C_1, C_2$  are constants.

**Theorem 2.** Let  $\mathcal{L}$  be any loss function satisfying the conditions in Lemma 1. Under class dependent noise, when the probability of the noise not changing the label is larger than changing it to another class ( $\eta_{ij} < 1 - \eta_{ii}$  for all  $i, j \in \{1, 2, \dots, K\}$ , with  $i \neq j$ ), and if  $R_{\mathcal{L}}^{\eta}(f^*) = 0$ , then

$$0 \leq R_{\mathcal{L}}^{\eta}(f^*) - R_{\mathcal{L}}^{\eta}(f_{\eta}) \leq (B_U - B_L) \mathbb{E}_{\mathcal{D}}[(1 - \eta_y)] + (C_1 - C_2) \mathbb{E}_{\mathcal{D}} \left[ \sum_{i \neq y}^K (1 - \eta_y - \eta_{yi}) \right], \quad (8)$$

where  $B_L \leq \sum_{i=1}^K \mathcal{L}(\mathbf{e}^{(i)}, \mathbf{x}, f) \leq B_U$  for all  $\mathbf{x}$  and  $f$ ,  $f^*$  is the global minimizer of  $R_{\mathcal{L}}(f)$ , and  $f_{\eta}^*$  is the global minimizer of  $R_{\mathcal{L}}^{\eta}(f)$ .

*Proof of Theorem 2.* For class dependent noisy(asymmetric) and any function,  $f$ , mapping an input  $\mathbf{x} \in \mathbb{X}$  to  $\Delta^{K-1}$ , we have

$$\begin{aligned}
R_{\mathcal{L}}^{\eta}(f) &= \mathbb{E}_{\mathcal{D}}[(1 - \eta_{yy})\mathcal{L}(\mathbf{e}^{(y)}, \mathbf{x}, f)] + \mathbb{E}_{\mathcal{D}}[\sum_{i \neq y}^K \eta_{yi} \mathcal{L}(\mathbf{e}^{(i)}, \mathbf{x}, f)] \\
&= \mathbb{E}_{\mathcal{D}}[(1 - \eta_{yy}) \left( \sum_{i=1}^K \mathcal{L}(\mathbf{e}^{(i)}, \mathbf{x}, f) - \sum_{i \neq y}^K \mathcal{L}(\mathbf{e}^{(i)}, \mathbf{x}, f) \right)] + \mathbb{E}_{\mathcal{D}}[\sum_{i \neq y}^K \eta_{yi} \mathcal{L}(\mathbf{e}^{(i)}, \mathbf{x}, f)] \\
&= \mathbb{E}_{\mathcal{D}}[(1 - \eta_{yy}) \sum_{i=1}^K \mathcal{L}(\mathbf{e}^{(i)}, \mathbf{x}, f)] - \mathbb{E}_{\mathcal{D}}[\sum_{i \neq y}^K (1 - \eta_y - \eta_{yi}) \mathcal{L}(\mathbf{e}^{(i)}, \mathbf{x}, f)]
\end{aligned}$$

By using the bounds  $B_L, B_U$  we get

$$\begin{aligned}
R_{\mathcal{L}}^{\eta}(f) &\leq B_U \mathbb{E}_{\mathcal{D}}[(1 - \eta_{yy})] - \mathbb{E}_{\mathcal{D}}[\sum_{i \neq y}^K (1 - \eta_y - \eta_{yi}) \mathcal{L}(\mathbf{e}^{(i)}, \mathbf{x}, f)] \\
R_{\mathcal{L}}^{\eta}(f) &\geq B_L \mathbb{E}_{\mathcal{D}}[(1 - \eta_y)] - \mathbb{E}_{\mathcal{D}}[\sum_{i \neq y}^K (1 - \eta_y - \eta_{yi}) \mathcal{L}(\mathbf{e}^{(i)}, \mathbf{x}, f)]
\end{aligned}$$

Hence,

$$\begin{aligned}
R_{\mathcal{L}}^{\eta}(f^*) - R_{\mathcal{L}}^{\eta}(f_{\eta}^*) &\leq (B_U - B_L) \mathbb{E}_{\mathcal{D}}[(1 - \eta_y)] + \\
&\quad + \mathbb{E}_{\mathcal{D}}[\sum_{i \neq y}^K (1 - \eta_y - \eta_{yi}) (\mathcal{L}(\mathbf{e}^{(i)}, \mathbf{x}, f_{\eta}^*) - \mathcal{L}(\mathbf{e}^{(i)}, \mathbf{x}, f^*))]
\end{aligned} \tag{9}$$

From the assumption that  $R_{\mathcal{L}}(f^*) = 0$ , we have  $\mathcal{L}(\mathbf{e}^{(y)}, \mathbf{x}, f^*) = 0$ . Using the conditions on the loss function from Lemma 1, for all  $i \neq y$ , we get

$$\begin{aligned}
\mathcal{L}(\mathbf{e}^{(i)}, \mathbf{x}, f_{\eta}^*) - \mathcal{L}(\mathbf{e}^{(i)}, \mathbf{x}, f^*) &= / \mathcal{L}(\mathbf{e}^{(y)}, \mathbf{x}, f^*) = 0 \text{ and } i / \\
&= \mathcal{L}(\mathbf{e}^{(i)}, \mathbf{x}, f_{\eta}^*) - \mathcal{L}(\mathbf{e}^{(i)}, \mathbf{e}^{(y)}) \\
&= / iii) / \\
&= \mathcal{L}(\mathbf{e}^{(i)}, \mathbf{x}, f_{\eta}^*) - C_2 \\
&= / ii) / \\
&\leq C_1 - C_2
\end{aligned}$$

By our assumption on the noise rates, we have  $(1 - \eta_{yy} - \eta_{yi}) > 0$ . We have

$$R_{\mathcal{L}}^{\eta}(f^*) - R_{\mathcal{L}}^{\eta}(f_{\eta}^*) \leq (B_U - B_L) \mathbb{E}_{\mathcal{D}}[(1 - \eta_{yy})] + (C_1 - C_2) \mathbb{E}_{\mathcal{D}}[\sum_{i \neq y}^K (1 - \eta_y - \eta_{yi})]$$

Since  $f_{\eta}^*$  is the global minimizer of  $R_{\mathcal{L}}^{\eta}(f)$  we have  $R_{\mathcal{L}}^{\eta}(f^*) - R_{\mathcal{L}}^{\eta}(f_{\eta}^*) \geq 0$ , which is the lower bound.  $\square$

**Remark 2.** The generalized Jensen-Shannon Divergence satisfies the conditions in Lemma 1, with

$$C_1 = H(\boldsymbol{\pi}), \quad C_2 = H(\pi_1) + H(1 - \pi_1).$$

*Proof of Remark 2.* i). Follows directly from Jensen's inequality for the Shannon entropy. ii). The lower bound follows directly from Jensen's inequality for the non-negative Shannon entropy. The

upper bound is shown below

$$\begin{aligned}
D_{\text{GJS}_\pi}(\mathbf{p}^{(1)}, \mathbf{p}^{(2)}, \dots, \mathbf{p}^{(M)}) &= \sum_{j=1}^M \pi_j D_{\text{KL}}(\mathbf{p}^{(j)} \parallel \mathbf{m}) \\
&= \sum_{j=1}^M \left[ \pi_j \sum_{l=1}^K p_l^{(j)} \log \left( \frac{p_l^{(j)}}{m_l} \right) \right] \\
&= \sum_{j=1}^M \left[ \pi_j \sum_{l=1}^K p_l^{(j)} \left( \log \left( \frac{\pi_j p_l^{(j)}}{m_l} \right) + \log \frac{1}{\pi_j} \right) \right] \\
&= \sum_{j=1}^M \left[ \pi_j \sum_{l=1}^K \left[ p_l^{(j)} \log \left( \frac{\pi_j p_l^{(j)}}{m_l} \right) - p_l^{(j)} \log \pi_j \right] \right] \\
&= \sum_{j=1}^M \left[ -\pi_j \log \pi_j + \pi_j \sum_{l=1}^K p_l^{(j)} \log \left( \frac{\pi_j p_l^{(j)}}{m_l} \right) \right] \\
&= \sum_{j=1}^M \left[ H(\pi_j) + \pi_j \sum_{l=1}^K p_l^{(j)} \log \left( \frac{\pi_j p_l^{(j)}}{m_l} \right) \right] \\
&= \sum_{j=1}^M \left[ H(\pi_j) + \pi_j \sum_{l=1}^K p_l^{(j)} \log \left( \frac{p_l^{(j)}}{p_l^{(j)} + \frac{1}{\pi_j} \sum_{i \neq j}^M \pi_i p_l^{(i)}} \right) \right] \\
&\leq \sum_{j=1}^M H(\pi_j) = H(\boldsymbol{\pi})
\end{aligned}$$

where the inequality holds with equality iff  $\frac{1}{\pi_j} \sum_{i \neq j}^M \pi_i p_l^{(i)} = 0$  when  $p_l^{(j)} > 0$  for all  $j \in \{1, 2, \dots, M\}$  and  $l \in \{1, 2, \dots, K\}$ . Hence, GJS is bounded above by  $H(\boldsymbol{\pi})$ .

iii). Let the label be  $\mathbf{e}^{(i)}$  and the other M-1 distributions be  $\mathbf{e}^{(j)}$  with  $i \neq j$  then

$$D_{\text{GJS}_\pi} = H(\pi_1 \mathbf{e}^{(i)} + \sum_{l=2}^M \pi_l \mathbf{e}^{(j)}) - \pi_1 H(\mathbf{e}^{(i)}) - \sum_{l=2}^M \pi_l H(\mathbf{e}^{(j)}) = H(\pi_1 \mathbf{e}^{(i)} + (1 - \pi_1) \mathbf{e}^{(j)}) \tag{10}$$

Notably,  $C_1 = C_2$  for  $M = 2$ .  $\square$

## C.2 Bounds

In this section, we first introduce some useful definitions and relate them to JS. Then, the bounds for JS and GJS are proven.

### C.2.1 Another Definition of Jensen-Shannon divergence

$$f_{\pi_1}(t) := \left[ H(\pi_1 t + 1 - \pi_1) - \pi_1 H(t) \right], t > 0 \tag{11}$$

$$f_{\pi_1}(0) := \lim_{t \rightarrow 0} f_{\pi_1}(t) \tag{12}$$

$$0f_{\pi_1}\left(\frac{0}{0}\right) := 0, \tag{13}$$

$$0f_{\pi_1}(0) := 0 \tag{14}$$

**Remark 3.** The Jensen-Shannon divergence can be rewritten using Equation 11 as follows

$$D_{\text{JS}_\pi}(\mathbf{p}^{(1)}, \mathbf{p}^{(2)}) = \sum_{k=1}^K p_k^{(2)} f_{\pi_1} \left( \frac{p_k^{(1)}}{p_k^{(2)}} \right) \tag{15}$$

*Proof of Remark 3.*

$$\sum_{k=1}^K p_k^{(2)} f_{\pi_1} \left( \frac{p_k^{(1)}}{p_k^{(2)}} \right) = \sum_{k=1}^K p_k^{(2)} \left[ \pi \frac{p_k^{(1)}}{p_k^{(2)}} \log \left( \frac{p_k^{(1)}}{p_k^{(2)}} \right) - \left( \pi \frac{p_k^{(1)}}{p_k^{(2)}} + 1 - \pi \right) \log \left( \pi \frac{p_k^{(1)}}{p_k^{(2)}} + 1 - \pi \right) \right] \quad (16)$$

$$= \sum_{k=1}^K \pi p_k^{(1)} \log \left( \frac{p_k^{(1)}}{p_k^{(2)}} \right) - \left( \pi p_k^{(1)} + (1 - \pi) p_k^{(2)} \right) \log \left( \frac{\pi p_k^{(1)} + (1 - \pi) p_k^{(2)}}{p_k^{(2)}} \right) \quad (17)$$

$$= \sum_{k=1}^K \pi p_k^{(1)} \log \left( \frac{p_k^{(1)}}{p_k^{(2)}} \right) - \pi p_k^{(1)} \log \left( \frac{\pi p_k^{(1)} + (1 - \pi) p_k^{(2)}}{p_k^{(2)}} \right) - (1 - \pi) p_k^{(2)} \log \left( \frac{\pi p_k^{(1)} + (1 - \pi) p_k^{(2)}}{p_k^{(2)}} \right) \quad (18)$$

$$= \sum_{k=1}^K \pi p_k^{(1)} \log \left( \frac{p_k^{(1)}}{\pi p_k^{(1)} + (1 - \pi) p_k^{(2)}} \right) + (1 - \pi) p_k^{(2)} \log \left( \frac{p_k^{(2)}}{\pi p_k^{(1)} + (1 - \pi) p_k^{(2)}} \right) \quad (19)$$

$$= \sum_{k=1}^K \pi D_{\text{KL}} \left( p_k^{(1)}, \pi p_k^{(1)} + (1 - \pi) p_k^{(2)} \right) + (1 - \pi) D_{\text{KL}} \left( p_k^{(2)}, \pi p_k^{(1)} + (1 - \pi) p_k^{(2)} \right) \quad (20)$$

$$= D_{\text{JS}}(\mathbf{p}^{(1)}, \mathbf{p}^{(2)}) \quad (21)$$

□

### C.2.2 Bounds for JS

**Proposition 4.**  $\mathcal{L}_{\text{JS}}$  has  $B_L \leq \sum_{k=1}^K \mathcal{L}_{\text{JS}}(\mathbf{e}^{(k)}, f(\mathbf{x})) \leq B_U$  with

$$B_L = \sum_{k=1}^K \mathcal{L}_{\text{JS}}(\mathbf{e}^{(k)}, \mathbf{u}), \quad B_U = \sum_{k=1}^K \mathcal{L}_{\text{JS}}(\mathbf{e}^{(k)}, \mathbf{e}^{(1)})$$

where  $\mathbf{u}$  is the uniform distribution.

*Proof of Proposition 4.*

First we start with two observations: 1)  $\sum_{k=1}^K \mathcal{L}_{\text{JS}}(\mathbf{e}^{(k)}, \mathbf{p})$  is strictly convex. 2)  $\sum_{k=1}^K \mathcal{L}_{\text{JS}}(\mathbf{e}^{(k)}, \mathbf{p})$  is invariant to permutations of the components of  $\mathbf{p}$ .

First, we show Observation 1). This is done by using Remark 3 and showing that the second derivatives are larger than zero

$$f_{\pi_1}(t) := \left[ H(\pi_1 t + 1 - \pi_1) - \pi_1 H(t) \right], t > 0 \quad (22)$$

$$f'_{\pi_1}(t) = \left[ \pi_1 (-\log(\pi_1 t + 1 - \pi_1) + \log(t)) \right] \quad (23)$$

$$f''_{\pi_1}(t) = \frac{\pi_1(1 - \pi_1)}{\pi_1 t^2 + t(1 - \pi_1)} \quad (24)$$

Hence,  $f_{\pi_1}(t)$  is strictly convex, since  $\pi_1 > 0$  and  $t > 0$ , then  $f''_{\pi_1}(t) > 0$ . With Remark 3, and that the sum of strictly convex functions is also strictly convex, it follows that  $\sum_{k=1}^K \mathcal{L}_{\text{JS}}(\mathbf{e}^{(k)}, \mathbf{p})$  is strictly convex.

Next, we show Observation 2), i.e., that  $\sum_{k=1}^K \mathcal{L}_{\text{JS}}(\mathbf{e}^{(k)}, \mathbf{p})$  is invariant to permutations of  $\mathbf{p}$

$$\sum_{k=1}^K D_{\text{JS}}(\mathbf{e}^{(k)}, \mathbf{p}) = \sum_{k=1}^K \left[ H(\pi_1 \mathbf{e}^{(k)} + \pi_2 \mathbf{p}) - \pi_2 H(\mathbf{p}) \right] \quad (25)$$

$$= \sum_{k=1}^K \left[ H(\pi_1 + \pi_2 p_k) + \sum_{i \neq k}^K H(\pi_2 p_i) - \pi_2 H(\mathbf{p}) \right] \quad (26)$$

$$= \sum_{k=1}^K H(\pi_1 + \pi_2 p_k) + \sum_{k=1}^K \sum_{i \neq k}^K H(\pi_2 p_i) - \pi_2 K H(\mathbf{p}) \quad (27)$$

$$= \sum_{k=1}^K H(\pi_1 + \pi_2 p_k) + \sum_{k=1}^K \left[ H(\pi_2 \mathbf{p}) - H(\pi_2 p_k) \right] - \pi_2 K H(\mathbf{p}) \quad (28)$$

$$= \sum_{k=1}^K H(\pi_1 + \pi_2 p_k) + (K-1) H(\pi_2 \mathbf{p}) - \pi_2 K H(\mathbf{p}) \quad (29)$$

$$= \sum_{k=1}^K H(\pi_1 + \pi_2 p_k) + (K-1) (H(\pi_2) + \pi_2 H(\mathbf{p})) - \pi_2 K H(\mathbf{p}) \quad (30)$$

$$= \sum_{k=1}^K H(\pi_1 + \pi_2 p_k) + (K-1) H(\pi_2) - \pi_2 H(\mathbf{p}) \quad (31)$$

Clearly, a permutation of the components of  $\mathbf{p}$  does not change the first sum or  $H(\mathbf{p})$ , since it would simply reorder the summands. Hence,  $\sum_{k=1}^K \mathcal{L}_{\text{JS}}(\mathbf{e}^{(k)}, \mathbf{p})$  is invariant to permutations of  $\mathbf{p}$ .

**Lower bound:**

The minimizer of a strictly convex function  $\left( \sum_{k=1}^K \mathcal{L}_{\text{JS}}(\mathbf{e}^{(k)}, \mathbf{p}) \right)$  over a compact convex set  $(\Delta^{K-1})$  is unique. Since  $\mathbf{u}$  is the only element of  $\Delta^{K-1}$  that is the same under permutation, it is the unique minimum of  $\sum_{k=1}^K \mathcal{L}_{\text{JS}}(\mathbf{e}^{(k)}, \mathbf{p})$  for  $\mathbf{p} \in \Delta^{K-1}$ .

**Upper bound:**

The maximizer of a strictly convex function  $\left( \sum_{k=1}^K \mathcal{L}_{\text{JS}}(\mathbf{e}^{(k)}, \mathbf{p}) \right)$  over a compact convex set  $(\Delta^{K-1})$  is at its extreme points  $(\mathbf{e}^{(i)} \text{ for } i \in \{1, 2, \dots, K\})$ . All extreme points have the same value according to Observation 2).

□

### C.2.3 Bounds for GJS

**Proposition 3.** GJS loss with  $M \leq K+1$  satisfies  $B_L \leq \sum_{k=1}^K \mathcal{L}_{\text{GJS}}(\mathbf{e}^{(k)}, \mathbf{p}^{(2)}, \dots, \mathbf{p}^{(M)}) \leq B_U$  for all  $\mathbf{p}^{(2)}, \dots, \mathbf{p}^{(M)} \in \Delta^{K-1}$ , with the following bounds

$$B_L = \sum_{k=1}^K \mathcal{L}_{\text{GJS}}(\mathbf{e}^{(k)}, \mathbf{u}, \dots, \mathbf{u}), \quad B_U = \sum_{k=1}^K \mathcal{L}_{\text{GJS}}(\mathbf{e}^{(k)}, \mathbf{e}^{(1)}, \dots, \mathbf{e}^{(M-1)}) \quad (6)$$

*Proof of Proposition 3.*

**Lower bound:** Using Proposition 2 to rewrite GJS into a JS and a consistency term, we get

$$\sum_{k=1}^K D_{\text{GJS}_{\pi}}(\mathbf{e}^{(k)}, \mathbf{p}^{(2)}, \dots, \mathbf{p}^{(M)}) = \sum_{k=1}^K \left[ D_{\text{JS}_{\pi'}}(\mathbf{e}^{(k)}, \mathbf{m}_{>1}) + (1 - \pi_1) D_{\text{GJS}_{\pi''}}(\mathbf{p}^{(2)}, \dots, \mathbf{p}^{(M)}) \right] \quad (32)$$

$$= \sum_{k=1}^K D_{\text{JS}_{\pi'}}(\mathbf{e}^{(k)}, \mathbf{m}_{>1}) + (1 - \pi_1) K D_{\text{GJS}_{\pi''}}(\mathbf{p}^{(2)}, \dots, \mathbf{p}^{(M)}) \quad (33)$$

$$\geq \sum_{k=1}^K D_{\text{JS}_{\pi'}}(\mathbf{e}^{(k)}, \mathbf{u}) + (1 - \pi_1) K D_{\text{GJS}_{\pi''}}(\mathbf{p}^{(2)}, \dots, \mathbf{p}^{(M)}) \quad (34)$$

$$\geq \sum_{k=1}^K D_{\text{JS}_{\pi'}}(\mathbf{e}^{(k)}, \mathbf{u}) \quad (35)$$

where the first inequality comes from the lower bound of Proposition 4, and the second inequality comes from

$(1 - \pi_1) K D_{\text{GJS}_{\pi''}}(\mathbf{p}^{(2)}, \dots, \mathbf{p}^{(M)})$  being non-negative. The inequalities holds with equality if and only if

$\mathbf{p}^{(2)} = \dots = \mathbf{p}^{(M)} = \mathbf{u}$ . Notably, the lower bound of JS is the same as that of GJS.

**Upper bound:**

Let's denote  $A(\mathbf{p}^{(2)}, \dots, \mathbf{p}^{(M)}) = \sum_{k=1}^K \mathcal{L}_{\text{GJS}}(\mathbf{e}^{(k)}, \mathbf{p}^{(2)}, \dots, \mathbf{p}^{(M)})$ . First we start by making 5 observations:

Observation 1:  $\Delta_{M-1}^{K-1} = \Delta^{K-1} \times \Delta^{K-1} \times \dots \times \Delta^{K-1}$  is a compact convex set.

Observation 2:  $A$  is strictly convex over  $\Delta_{M-1}^{K-1}$ .

Observation 3: From Observations 1 and 2 we have that the maximizer of  $A$  should be at extreme points of  $\Delta_{M-1}^{K-1}$ , i.e., a unit vector in every  $M-1$  individual  $\Delta^{K-1}$  subspaces of  $\Delta_{M-1}^{K-1}$ .

Observation 4:  $A$  is symmetric w.r.t. permutations of the components of predictive distributions  $\mathbf{p}^{(i)}$ .

Unlike for JS, the extreme points of  $\Delta_{M-1}^{K-1}$  do not necessarily map to the same value of  $A$ . Hence, what is left to show is that the set of extreme points with all predictive distributions being *distinct* unit vectors maps to the maximum value of  $A$ .

Given Observation 3, all the  $M$  distributions are unit vectors, therefore the maximum is of the form  $A(\mathbf{p}^{(2)}, \dots, \mathbf{p}^{(M)}) = \sum_{k=1}^K H(\pi_1 \mathbf{e}^{(k)} + (1 - \pi_1) \mathbf{m}_{>1})$ , where  $\mathbf{m}_{>1} := \sum_{j=2}^M \pi_j \mathbf{p}^{(j)} / (1 - \pi_1)$ . Furthermore, at most  $M-1$  components of  $\mathbf{m}_{>1}$  are non-zero (if all predictions are distinct). From Observation 4, we can WLOG permute  $\mathbf{m}_{>1}$  such that the first  $M-1$  components are the largest ones. Let  $\mathbf{m}_{>1}^C \in \Delta^{M-2}$  denote the subset of these first  $M-1$  components of  $\mathbf{m}_{>1} \in \Delta^{K-1}$ . Then, for all predictive distributions being unit vectors, we have

$$A(\mathbf{p}^{(2)}, \dots, \mathbf{p}^{(M)}) = \sum_{k=1}^K H(\pi_1 \mathbf{e}^{(k)} + (1 - \pi_1) \mathbf{m}_{>1}) \quad (36)$$

$$= \sum_{k=1}^{M-1} \left[ H(\pi_1 + (1 - \pi_1) m_{>1,k}) + (K-1) H((1 - \pi_1) m_{>1,k}) \right] + \sum_{k=M}^K H(\pi_1) \quad (37)$$

$$= \sum_{k=1}^{M-1} H(\pi_1 + (1 - \pi_1) m_{>1,k}) + (K-1) H((1 - \pi_1) \mathbf{m}_{>1}^C) + \sum_{k=M}^K H(\pi_1) \quad (38)$$

$$\leq (M-1) H\left(\frac{1}{M-1} \sum_{k=1}^{M-1} [\pi_1 + (1 - \pi_1) m_{>1,k}] \right) + (K-1) H((1 - \pi_1) \mathbf{m}_{>1}^C) + \sum_{k=M}^K H(\pi_1) \quad (39)$$

$$= (M-1) H\left(\pi_1 + \frac{1 - \pi_1}{M-1}\right) + (K-1) H((1 - \pi_1) \mathbf{m}_{>1}^C) + \sum_{k=M}^K H(\pi_1) \quad (40)$$

$$\leq (M-1) H\left(\pi_1 + \frac{1 - \pi_1}{M-1}\right) + (K-1) H((1 - \pi_1) \mathbf{u}) + \sum_{k=M}^K H(\pi_1) \quad (41)$$

The first inequality follows from Jensen's inequality and the second from the uniform distribution maximizes entropy. Both inequalities hold with equality iff  $m_{>1,1} = \dots = m_{>1,M-1}$ . Hence, the maximum is achieved if  $\mathbf{m}_{>1}^C = \mathbf{u} \in \Delta^{M-2}$ , which is only possible if all  $M-1$  predictive distributions are distinct unit vectors.

□

### C.3 Robustness of Jensen-Shannon losses

In this section, we prove that the lower ( $B_L$ ) and upper ( $B_U$ ) bounds become the same for JS and GJS as  $\pi_1 \rightarrow 1$  as stated in Remark 1.

**Remark 1.**  $\mathcal{L}_{\text{JS}}$  and  $\mathcal{L}_{\text{GJS}}$  are robust ( $B_L = B_U$ ) in the limit of  $\pi_1 \rightarrow 1$ .

*Proof of Remark 1 for JS.*

**Lower bound:**

$$\sum_{k=1}^K D_{\text{JS},\pi}(\mathbf{e}^{(y)}, \mathbf{u}) = \sum_{k=1}^K H(\pi_1 \mathbf{e}^{(k)} + \pi_2 \mathbf{u}) - \pi_2 H(\mathbf{u}) \quad (42)$$

$$= K[H(\pi_1 \mathbf{e}^{(1)} + \pi_2 \mathbf{u}) - \pi_2 H(\mathbf{u})] \quad (43)$$

$$= K[H(\pi_1 + \pi_2/K) + (K-1)H(\pi_2/K) - K\pi_2 H(\frac{1}{K})] \quad (44)$$

$$= /H(\pi_2/K) = -\pi_2/K(\log \pi_2 + \log 1/K) = \frac{1}{K}H(\pi_2) + \pi_2 H(1/K)/ \quad (45)$$

$$= K[H(\pi_1 + \pi_2/K) + (K-1)(\frac{1}{K}H(\pi_2) + \pi_2 H(\frac{1}{K})) - K\pi_2 H(\frac{1}{K})] \quad (46)$$

$$= K[H(\pi_1 + \pi_2/K) + (K-1)\frac{1}{K}H(\pi_2) - \pi_2 H(\frac{1}{K})] \quad (47)$$

If one now normalize ( $Z = H(\pi_2) = H(1 - \pi_1)$ ) and take the limit as  $\pi_1 \rightarrow 1$  we get:

$$\lim_{\pi_1 \rightarrow 1} \sum_{k=1}^K \mathcal{L}_{\text{JS}}(\mathbf{e}^{(y)}, \mathbf{u}) = \lim_{\pi_1 \rightarrow 1} (K-1) + K \frac{H(\pi_1 + \pi_2/K) - \pi_2 H(\frac{1}{K})}{H(\pi_2)} \quad (48)$$

$$= \lim_{\pi_1 \rightarrow 1} (K-1) + K \frac{-(K-1)(1 + \log(\pi_1 + \pi_2/K))/K - \log(1/K)/K}{\log(1 - \pi_1) + 1} \quad (49)$$

$$= \lim_{\pi_1 \rightarrow 1} (K-1) - \frac{(K-1)(1 + \log(\pi_1 + \pi_2/K)) - \log(1/K)}{\log(1 - \pi_1) + 1} \quad (50)$$

$$= \lim_{\pi_1 \rightarrow 1} (K-1) - ((K-1)(1 + \log(\pi_1 + \pi_2/K)) - \log(1/K)) \frac{1}{\log(1 - \pi_1) + 1} \quad (51)$$

$$= (K-1) - (K-1 - \log(1/K)) \cdot 0 \quad (52)$$

$$= K-1 \quad (53)$$

where L'Hôpital's rule was used for the fraction in Equation 48 which is indeterminate of the form  $\frac{0}{0}$ .

**Upper bound:**

$$\sum_{k=1}^K \mathcal{L}_{\text{JS}}(\mathbf{e}^{(k)}, \mathbf{e}^{(1)}) = \frac{1}{H(\pi_2)} \sum_{k=1}^K H(\pi_1 \mathbf{e}^{(k)} + \pi_2 \mathbf{e}^{(1)}) \quad (54)$$

$$= \frac{1}{H(\pi_2)} [(K-1)H(\pi_2) + (K-1)H(\pi_1) + H(\pi_1 + \pi_2)] \quad (55)$$

$$= (K-1)[1 + \frac{H(\pi_1)}{H(\pi_2)}] \quad (56)$$

$$= (K-1) \left[ 1 + \frac{\pi_1 \log \pi_1}{(1 - \pi_1) \log(1 - \pi_1)} \right] \quad (57)$$

Taking the limit as  $\pi_1 \rightarrow 1$  gives

$$\lim_{\pi_1 \rightarrow 1} \sum_{k=1}^K \mathcal{L}_{\text{JS}}(\mathbf{e}^{(k)}, \mathbf{e}^{(1)}) = \lim_{\pi_1 \rightarrow 1} (K-1) \left[ 1 + \pi_1 \frac{1}{\log(1-\pi_1)} \frac{\log \pi_1}{(1-\pi_1)} \right] \quad (58)$$

$$= \lim_{\pi_1 \rightarrow 1} (K-1) \left[ 1 + \pi_1 \frac{1}{\log(1-\pi_1)} \frac{1}{\pi_1} \frac{1}{-1} \right] \quad (59)$$

$$= (K-1)[1 + 1 \cdot 0 \cdot 1 \cdot -1] \quad (60)$$

$$= K-1 \quad (61)$$

where L'Hôpital's rule was used for  $\lim_{\pi_1 \rightarrow 1} \frac{\log \pi_1}{(1-\pi_1)}$  which is indeterminate of the form  $\frac{0}{0}$ . Hence,  $B_L = B_U = K-1$ .  $\square$

Next, we look at the robustness of the generalized Jensen-Shannon loss.

*Proof of Remark 1 for GJS.*

Proposition 2, shows that GJS can be rewritten as a JS term and a consistency term. From the proof of Remark 1 for JS above, it follows that the JS term satisfies  $B_L = B_U$  as  $\pi_1$  approaches 1. Hence, it is enough to show that the consistency term of GJS also becomes a constant in this limit. The consistency term is the generalized Jensen-Shannon divergence

$$\lim_{\pi_1 \rightarrow 1} (1-\pi_1) \mathcal{L}_{\text{GJS}_{\pi''}}(\mathbf{p}^{(2)}, \dots, \mathbf{p}^{(M)}) = \lim_{\pi_1 \rightarrow 1} \frac{(1-\pi_1)}{H(1-\pi_1)} D_{\text{GJS}_{\pi''}}(\mathbf{p}^{(2)}, \dots, \mathbf{p}^{(M)}) \quad (62)$$

$$= \lim_{\pi_1 \rightarrow 1} -\frac{1}{\log(1-\pi_1)} D_{\text{GJS}_{\pi''}}(\mathbf{p}^{(2)}, \dots, \mathbf{p}^{(M)}) \quad (63)$$

$$= 0 \quad (64)$$

where  $\pi'' = [\pi_2, \dots, \pi_M]/(1-\pi_1)$ .  $D_{\text{GJS}_{\pi''}}(\mathbf{p}^{(2)}, \dots, \mathbf{p}^{(M)})$  is bounded and  $-\frac{1}{\log(1-\pi_1)}$  goes to zero as  $\pi_1 \rightarrow 1$ , hence the limit of the product goes to zero.  $\square$

#### C.4 Connection to JS and Consistency

**Proposition 2.** Let  $\mathbf{p}^{(2)}, \dots, \mathbf{p}^{(M)} \in \Delta^{K-1}$  with  $M \geq 3$  and  $\mathbf{m}_{>1} = \frac{\sum_{j=2}^M \pi_j \mathbf{p}^{(j)}}{1-\pi_1}$ , then

$$\mathcal{L}_{\text{GJS}}(\mathbf{e}^{(y)}, \mathbf{p}^{(2)}, \dots, \mathbf{p}^{(M)}) = \mathcal{L}_{\text{JS}_{\pi'}}(\mathbf{e}^{(y)}, \mathbf{m}_{>1}) + (1-\pi_1) \mathcal{L}_{\text{GJS}_{\pi''}}(\mathbf{p}^{(2)}, \dots, \mathbf{p}^{(M)})$$

where  $\pi' = [\pi_1, 1-\pi_1]^T$  and  $\pi'' = \frac{[\pi_2, \dots, \pi_M]^T}{(1-\pi_1)}$ .

*Proof of Proposition 2.* The Generalized Jensen-Shannon divergence can be simplified as below

$$\text{GJS}_{\boldsymbol{\pi}}(\mathbf{e}^{(y)}, \mathbf{p}^{(2)}, \dots, \mathbf{p}^{(M)}) = H(\pi_1 \mathbf{e}^{(y)} + (1 - \pi_1) \mathbf{m}_{>1}) - \sum_{j=2}^M \pi_j H(\mathbf{p}^{(j)}) \quad (65)$$

$$= H(\pi_1 + (1 - \pi_1)m_y) + \sum_{i \neq y}^K H((1 - \pi_1)m_i) - \sum_{j=2}^M \pi_j H(\mathbf{p}^{(j)}) \quad (66)$$

$$= / H(\pi_2 p_i) = p_i H(\pi_2) + \pi_2 H(p_i) / \quad (67)$$

$$= H(\pi_1 + (1 - \pi_1)m_y) + \sum_{i \neq y}^K [m_i H(1 - \pi_1) + (1 - \pi_1)H(m_i)] - \sum_{j=2}^M \pi_j H(\mathbf{p}^{(j)}) \quad (68)$$

$$= H(\pi_1 + (1 - \pi_1)m_y) + \sum_{i \neq y}^K [m_i H(1 - \pi_1)] - (1 - \pi_1)H(m_y) \quad (69)$$

$$+ (1 - \pi_1) \left( H(\mathbf{m}_{>1}) - \frac{1}{1 - \pi_1} \sum_{j=2}^M \pi_j H(\mathbf{p}^{(j)}) \right) \quad (70)$$

$$= H(\pi_1 + (1 - \pi_1)m_y) + \sum_{i \neq y}^K [m_i H(1 - \pi_1) + (1 - \pi_1)(H(m_i) - H(m_y))] \quad (71)$$

$$- (1 - \pi_1)H(m_y) + (1 - \pi_1)D_{\text{GJS}_{\boldsymbol{\pi}''}}(\mathbf{p}^{(2)}, \dots, \mathbf{p}^{(M)}) \quad (72)$$

$$= / \text{Equation 67} / \quad (73)$$

$$= H(\pi_1 + (1 - \pi_1)m_y) + \sum_{i \neq y}^K H((1 - \pi_1)m_i) - (1 - \pi_1)H(\mathbf{m}_{>1}) \quad (74)$$

$$+ (1 - \pi_1)D_{\text{GJS}_{\boldsymbol{\pi}''}}(\mathbf{p}^{(2)}, \dots, \mathbf{p}^{(M)}) \quad (75)$$

$$= H(\pi_1 \mathbf{e}^{(y)} + (1 - \pi_1) \mathbf{m}_{>1}) - (1 - \pi_1)H(\mathbf{m}_{>1}) + (1 - \pi_1)D_{\text{GJS}_{\boldsymbol{\pi}''}}(\mathbf{p}^{(2)}, \dots, \mathbf{p}^{(M)}) \quad (76)$$

$$= D_{\text{JS}_{\boldsymbol{\pi}''}}(\mathbf{e}^{(y)}, \mathbf{m}_{>1}) + (1 - \pi_1)D_{\text{GJS}_{\boldsymbol{\pi}''}}(\mathbf{p}^{(2)}, \dots, \mathbf{p}^{(M)}) \quad (77)$$

where  $\boldsymbol{\pi}' = [\pi_1, 1 - \pi_1]$  and  $\boldsymbol{\pi}'' = [\pi_2, \dots, \pi_M]/(1 - \pi_1)$ .  $\square$

That is, when using onehot labels, the generalized Jensen-Shannon divergence is a combination of two terms, one term encourages the mean prediction to be similar to the label and another term that encourages consistency between the predictions. For  $M = 2$ , the consistency term is zero.

## C.5 Connection to CE and MAE

**Proposition 1.** Let  $\mathbf{p} \in \Delta^{K-1}$ , then

$$\lim_{\pi_1 \rightarrow 0} \mathcal{L}_{\text{JS}}(\mathbf{e}^{(y)}, \mathbf{p}) = H(\mathbf{e}^{(y)}, \mathbf{p}), \quad \lim_{\pi_1 \rightarrow 1} \mathcal{L}_{\text{JS}}(\mathbf{e}^{(y)}, \mathbf{p}) = \frac{1}{2} \|\mathbf{e}^{(y)} - \mathbf{p}\|_1 \quad (4)$$

where  $H(\mathbf{e}^{(y)}, \mathbf{p})$  is the cross entropy of  $\mathbf{e}^{(y)}$  relative to  $\mathbf{p}$ .

*Proof of Proposition 1.* We want to show

$$\lim_{\pi_1 \rightarrow 0} \mathcal{L}_{\text{JS}}(\mathbf{e}^{(y)}, \mathbf{p}) = \lim_{\pi_1 \rightarrow 0} \frac{\text{JS}_{\boldsymbol{\pi}}(\mathbf{e}^{(y)}, \mathbf{p})}{H(1 - \pi_1)} = H(\mathbf{e}^{(y)}, \mathbf{p}) \quad (78)$$

$$\lim_{\pi_1 \rightarrow 1} \mathcal{L}_{\text{JS}}(\mathbf{e}^{(y)}, \mathbf{p}) = \lim_{\pi_1 \rightarrow 1} \frac{\text{JS}_{\boldsymbol{\pi}}(\mathbf{e}^{(y)}, \mathbf{p})}{H(1 - \pi_1)} = \frac{1}{2} \|\mathbf{e}^{(y)} - \mathbf{p}\|_1 \quad (79)$$

More specifically, we have  $\text{JS}_{\pi}(\mathbf{e}^{(y)}, \mathbf{p}) = \pi_1 D_{\text{KL}}(\mathbf{e}^{(y)} \parallel \mathbf{m}) + \pi_2 D_{\text{KL}}(\mathbf{p} \parallel \mathbf{m})$ , where  $\mathbf{m} = \pi_1 \mathbf{e}^{(y)} + \pi_2 \mathbf{p}$ , and

$$\lim_{\pi_1 \rightarrow 0} \frac{\pi_1 D_{\text{KL}}(\mathbf{e}^{(y)} \parallel \mathbf{m})}{H(1 - \pi_1)} = H(\mathbf{e}^{(y)}, \mathbf{p}) \quad (80)$$

$$\lim_{\pi_1 \rightarrow 1} \frac{\pi_2 D_{\text{KL}}(\mathbf{p} \parallel \mathbf{m})}{H(1 - \pi_1)} = \frac{1}{2} \|\mathbf{e}^{(y)} - \mathbf{p}\|_1 \quad (81)$$

First, we prove Equations 80 and 81, then show that the other two limits are zero. Proof of Equation 80

$$\lim_{\pi_1 \rightarrow 0} \frac{\pi_1 D_{\text{KL}}(\mathbf{e}^{(y)} \parallel \mathbf{m})}{H(1 - \pi_1)} = \lim_{\pi_1 \rightarrow 0} \frac{-\pi_1 \log(m_y)}{-(1 - \pi_1) \log(1 - \pi_1)} \quad (82)$$

$$= \lim_{\pi_1 \rightarrow 0} \log(m_y) \frac{1}{1 - \pi_1} \frac{\pi_1}{\log(1 - \pi_1)} \quad (83)$$

$$= \lim_{\pi_1 \rightarrow 0} \log(m_y) \frac{1}{1 - \pi_1} \cdot -(1 - \pi_1) \quad (84)$$

$$= \log p_y \cdot 1 \cdot -1 = H(\mathbf{e}^{(y)}, \mathbf{p}^{(2)}) \quad (85)$$

where we used L'Hôpital's rule for  $\lim_{\pi_1 \rightarrow 0} \frac{\pi_1}{\log(1 - \pi_1)}$  which is indeterminate of the form  $\frac{0}{0}$ .

Proof of Equation 81

$$\lim_{\pi_1 \rightarrow 1} \frac{\pi_2 D_{\text{KL}}(\mathbf{p} \parallel \mathbf{m})}{H(1 - \pi_1)} = \lim_{\pi_1 \rightarrow 1} \frac{(1 - \pi_1)}{H(1 - \pi_1)} \sum_{k=1}^K p_k \log \frac{p_k}{m_k} \quad (86)$$

$$= \lim_{\pi_1 \rightarrow 1} -\frac{1}{\log(1 - \pi_1)} \sum_{k=1}^K p_k \log \frac{p_k}{m_k} \quad (87)$$

$$= \lim_{\pi_1 \rightarrow 1} -\frac{1}{\log(1 - \pi_1)} \left[ p_y \log \frac{p_y}{m_y} + \sum_{k \neq y}^K p_k \log \frac{p_k}{(1 - \pi_1)p_k} \right] \quad (88)$$

$$= \lim_{\pi_1 \rightarrow 1} -\frac{1}{\log(1 - \pi_1)} \left[ p_y \log \frac{p_y}{m_y} - \log(1 - \pi_1) \sum_{k \neq y}^K p_k \right] \quad (89)$$

$$= \lim_{\pi_1 \rightarrow 1} -\frac{1}{\log(1 - \pi_1)} \left[ p_y \log \frac{p_y}{m_y} - \log(1 - \pi_1)(1 - p_y) \right] \quad (90)$$

$$= \lim_{\pi_1 \rightarrow 1} -p_y \log \frac{p_y}{m_y} \frac{1}{\log(1 - \pi_1)} + 1 - p_y \quad (91)$$

$$= 0 \cdot 0 + 1 - p_y \quad (92)$$

$$= \frac{1}{2} (1 - p_y + 1 - p_y) \quad (93)$$

$$= \frac{1}{2} (1 - p_y + \sum_{k \neq y}^K p_k) \quad (94)$$

$$= \frac{1}{2} \sum_{k=1}^K \left| e_k^{(y)} - p_k \right| \quad (95)$$

$$= \frac{1}{2} \|\mathbf{e}^{(y)} - \mathbf{p}\|_1 \quad (96)$$

Now, what is left to show is that the last two terms goes to zero in their respective limits.

$$\lim_{\pi_1 \rightarrow 1} \frac{\pi_1 D_{\text{KL}}(\mathbf{e}^{(y)} \parallel \mathbf{m})}{H(1 - \pi_1)} = \lim_{\pi_1 \rightarrow 1} \frac{-\pi_1 \log(m_y)}{-(1 - \pi_1) \log(1 - \pi_1)} \quad (97)$$

$$= \lim_{\pi_1 \rightarrow 1} \frac{-\pi_1 \log(\pi_1 + (1 - \pi_1)p_y)}{-(1 - \pi_1) \log(1 - \pi_1)} \quad (98)$$

$$= \lim_{\pi_1 \rightarrow 1} \frac{\pi_1}{\log(1 - \pi_1)} \frac{\log(\pi_1 + (1 - \pi_1)p_y)}{1 - \pi_1} \quad (99)$$

$$= 0 \cdot (p_y - 1) = 0 \quad (100)$$

And the last term

$$\lim_{\pi_1 \rightarrow 0} \frac{\pi_2 D_{\text{KL}}(\mathbf{p}^{(2)} \parallel \mathbf{m})}{H(1 - \pi_1)} = / \text{ Equation 91 } / \quad (101)$$

$$= \lim_{\pi_1 \rightarrow 0} -p_y \log \frac{p_y}{m_y} \frac{1}{\log(1 - \pi_1)} + 1 - p_y \quad (102)$$

$$= \lim_{\pi_1 \rightarrow 0} -p_y \frac{\log \frac{p_y}{m_y}}{\log(1 - \pi_1)} + 1 - p_y \quad (103)$$

$$= \lim_{\pi_1 \rightarrow 0} -p_y \left( -\frac{1 - p_y}{\pi_1 + (1 - \pi_1)p_y} \cdot -(1 - \pi_1) \right) + 1 - p_y \quad (104)$$

$$= \lim_{\pi_1 \rightarrow 0} -p_y \left( \frac{(1 - p_y)(1 - \pi_1)}{\pi_1 + (1 - \pi_1)p_y} \right) + 1 - p_y \quad (105)$$

$$= \lim_{\pi_1 \rightarrow 0} p_y \left( \frac{-1 + \pi_1 + (1 - \pi_1)p_y}{\pi_1 + (1 - \pi_1)p_y} \right) + 1 - p_y \quad (106)$$

$$= \lim_{\pi_1 \rightarrow 0} p_y \left( \frac{-1}{\pi_1 + (1 - \pi_1)p_y} + 1 \right) + 1 - p_y \quad (107)$$

$$= -1 + p_y + 1 - p_y \quad (108)$$

$$= 0 \quad (109)$$

where L'Hôpital's rule was used for  $\lim_{\pi_1 \rightarrow 0} -p_y \frac{\log \frac{p_y}{m_y}}{\log(1 - \pi_1)}$  which is indeterminate of the form  $\frac{0}{0}$ .  $\square$

## C.6 Gradients of Jensen-Shannon Divergence

The partial derivative of the Jensen-Shannon divergence is

$$\frac{\partial \{H(\mathbf{m}) - \pi_1 H(\mathbf{e}^{(y)}) - (1 - \pi_1) H(\mathbf{p})\}}{\partial z_i}$$

where  $\mathbf{m} = \pi_1 \mathbf{e}^{(y)} + \pi_2 \mathbf{p} = \pi_1 \mathbf{e}^{(y)} + (1 - \pi_1) \mathbf{p}$ , and  $p_j = e^{z_j} / \sum_{k=1}^K e^{z_k}$ . Note the difference between  $e^z$  which is the exponential function while  $\mathbf{e}^{(y)}$  is a onehot label. We take the partial derivative of each term separately, but first the partial derivative of the  $j$ th component of a softmax

output with respect to the  $i$ th component of the corresponding logit

$$\frac{\partial p_j}{\partial z_i} = \frac{\partial}{\partial z_i} \frac{e^{z_j}}{\sum_{k=1}^K e^{z_k}} \quad (110)$$

$$= \frac{\frac{\partial e^{z_j}}{\partial z_i} \sum_{k=1}^K e^{z_k} - e^{z_j} \frac{\partial \sum_{k=1}^K e^{z_k}}{\partial z_i}}{\left( \sum_{k=1}^K e^{z_k} \right)^2} \quad (111)$$

$$= \frac{\mathbb{1}(i=j)e^{z_j} \sum_{k=1}^K e^{z_k} - e^{z_j} e^{z_i}}{\left( \sum_{k=1}^K e^{z_k} \right)^2} \quad (112)$$

$$= \frac{\mathbb{1}(i=j)e^{z_j} - p_j e^{z_i}}{\sum_{k=1}^K e^{z_k}} \quad (113)$$

$$= \mathbb{1}(i=j)p_j - p_j p_i \quad (114)$$

$$= p_j(\mathbb{1}(i=j) - p_i) \quad (115)$$

$$= p_i(\mathbb{1}(i=j) - p_j) \quad (116)$$

$$= \frac{\partial p_i}{\partial z_j} \quad (117)$$

where  $\mathbb{1}(i=j)$  is the indicator function, i.e., 1 when  $i = j$  and zero otherwise. Using the above, we get

$$\sum_{j=1}^K \frac{\partial p_j}{\partial z_i} = p_i \sum_{j=1}^K (\mathbb{1}(i=j) - p_j) = p_i(1 - 1) = 0 \quad (118)$$

First, the partial derivative of  $H(\mathbf{p})$  wrt  $z_i$

$$\frac{\partial H(\mathbf{p})}{\partial z_i} = - \sum_{j=1}^K \frac{\partial p_j \log p_j}{\partial z_i} \quad (119)$$

$$= - \sum_{j=1}^K \frac{\partial p_j}{\partial z_i} \log p_j + p_j \frac{\partial \log p_j}{\partial z_i} \quad (120)$$

$$= - \sum_{j=1}^K \frac{\partial p_j}{\partial z_i} \log p_j + p_j \frac{1}{p_j} \frac{\partial p_j}{\partial z_i} \quad (121)$$

$$= - \sum_{j=1}^K \frac{\partial p_j}{\partial z_i} (\log p_j + 1) \quad (122)$$

$$= / \text{Equation 118} / \quad (123)$$

$$= - \sum_{j=1}^K \frac{\partial p_j}{\partial z_i} \log p_j \quad (124)$$

Next, the partial derivative of  $H(\mathbf{m})$  wrt  $z_i$

$$\frac{\partial\{H(\mathbf{m})\}}{\partial z_i} = \frac{\partial\{\pi_1 H(\mathbf{e}^{(y)}, \mathbf{m}) + (1 - \pi_1) H(\mathbf{p}, \mathbf{m})\}}{\partial z_i} \quad (125)$$

$$= - \sum_{j=1}^K \left[ \pi_1 \frac{e_j^{(y)} \partial \log(m_j)}{\partial z_i} + (1 - \pi_1) \frac{\partial \{p_j \log(m_j)\}}{\partial z_i} \right] \quad (126)$$

$$= - \sum_{j=1}^K \left[ \pi_1 e_j^{(y)} \frac{\partial \log(m_j)}{\partial z_i} + (1 - \pi_1) \left( \frac{\partial p_j}{\partial z_i} \log(m_j) + p_j \frac{\partial \log(m_j)}{\partial z_i} \right) \right] \quad (127)$$

$$= - \sum_{j=1}^K \left[ m_j \frac{\partial \log(m_j)}{\partial z_i} + (1 - \pi_1) \frac{\partial p_j}{\partial z_i} \log(m_j) \right] \quad (128)$$

$$= - \sum_{j=1}^K \left[ (1 - \pi_1) \frac{\partial p_j}{\partial z_i} + (1 - \pi_1) \frac{\partial p_j}{\partial z_i} \log(m_j) \right] \quad (129)$$

$$= - \sum_{j=1}^K (1 - \pi_1) \frac{\partial p_j}{\partial z_i} \left[ 1 + \log(m_j) \right] = / \text{Equation 118} / \quad (130)$$

$$= - (1 - \pi_1) \sum_{j=1}^K \frac{\partial p_j}{\partial z_i} \log(m_j) \quad (131)$$

The partial derivative of the Jensen-Shannon divergence with respect to logit  $z_i$  is

$$\frac{\partial\{H(\mathbf{m}) - \pi_1 H(\mathbf{e}^{(y)}) - (1 - \pi_1) H(\mathbf{p})\}}{\partial z_i} = \frac{\partial\{H(\mathbf{m}) - (1 - \pi_1) H(\mathbf{p})\}}{\partial z_i} \quad (132)$$

$$= - (1 - \pi_1) \sum_{j=1}^K \frac{\partial p_j}{\partial z_i} \left( \log(m_j) - \log p_j \right) \quad (133)$$

$$= - (1 - \pi_1) \left[ \sum_{j=1}^K \frac{\partial p_j}{\partial z_i} \log \frac{m_j}{p_j} \right] \quad (134)$$

If we now make use of the fact that the label is  $\mathbf{e}^{(y)}$ , we can write the partial derivative wrt to  $z_i$  as

$$\frac{\partial\{H(\mathbf{m}) - \pi_1 H(\mathbf{e}^{(y)}) - (1 - \pi_1) H(\mathbf{p})\}}{\partial z_i} = \quad (135)$$

$$= - (1 - \pi_1) \left[ \sum_{j=1}^K \frac{\partial p_j}{\partial z_i} \log \left( \frac{\pi_1 e_j^{(y)}}{p_j} + (1 - \pi_1) \right) \right] \quad (136)$$

$$= - (1 - \pi_1) \left[ \frac{\partial p_y}{\partial z_i} \log \left( \frac{\pi_1}{p_y} + (1 - \pi_1) \right) + \sum_{j \neq y}^K \frac{\partial p_j}{\partial z_i} \log \left( 1 - \pi_1 \right) \right] \quad (137)$$

$$= - (1 - \pi_1) \left[ \frac{\partial p_y}{\partial z_i} \log \left( \frac{\pi_1}{p_y} + (1 - \pi_1) \right) + \log \left( 1 - \pi_1 \right) \sum_{j \neq y}^K \frac{\partial p_j}{\partial z_i} \right] \quad (138)$$

$$= \left/ \text{Eq 118} \Leftrightarrow \sum_{j \neq y}^K \frac{\partial p_j}{\partial z_i} = - \frac{\partial p_y}{\partial z_i} \right/ \quad (139)$$

$$= - (1 - \pi_1) \frac{\partial p_y}{\partial z_i} \left[ \log \left( \frac{\pi_1}{p_y} + (1 - \pi_1) \right) - \log \left( 1 - \pi_1 \right) \right] \quad (140)$$

$$= - (1 - \pi_1) \frac{\partial p_y}{\partial z_i} \log \left( \frac{\pi_1}{(1 - \pi_1)p_y} + 1 \right) \quad (141)$$

## D Extended Related Works

Most related to us is the avenue of handling noisy labels in deep learning via the identification and construction of *noise-robust loss functions* [2, 3, 4, 5]. Ghosh *et al.* [2] derived sufficient conditions for a loss function, in empirical risk minimization (ERM) settings, to be robust to various kinds of sample-independent noise, including symmetric, symmetric non-uniform, and class-conditional. They further argued that, while CE is not a robust loss function, mean absolute error (MAE) is a loss that satisfies the robustness conditions and empirically demonstrated its effectiveness. On the other hand, Zhang *et al.* [3] pointed out the challenges of training with MAE and proposed GCE which generalizes both MAE and CE losses. Tuning for this trade-off, GCE alleviates MAE’s training difficulties while retaining some desirable noise-robustness properties. In a similar fashion, symmetric cross entropy (SCE) [4] spans the spectrum of reverse CE as a noise-robust loss function and the standard CE. Recently, Ma *et al.* [5] proposed a normalization mechanism to make arbitrary loss functions robust to noise. They, too, further combine two complementary loss functions to improve the data fitting while keeping robust to noise. The current work extends on this line of works.

Several other directions are pursued to improve training of deep networks under noisy labelled datasets. This includes methods to *identify and remove* noisy labels [29, 30] or *identify and correct* noisy labels in a joint label-parameter optimization [31, 32] and those works that design an *elaborate training pipeline* for dealing with noise [15, 33, 34]. In contrast to these directions, this work proposes a robust loss function based on Jensen-Shannon divergence (JS) without altering other aspects of training. In the following, we review the directions that are most related to this paper.

A close line of works to ours *reweight a loss function* by a known or estimated class-conditional noise model [10]. This direction has been commonly studied for deep networks with a standard cross entropy (CE) loss [11, 12, 13, 14]. Assuming a class-conditional noise model, loss correction is theoretically well motivated.

A common regularization technique called *label smoothing* [35] has been recently proposed that operates similarly to the loss correction methods. While its initial purpose was for deep networks to avoid overfitting, label smoothing has been shown to have a noticeable effect when training with noisy sets by alleviating the fit to the noise [19, 20].

*Consistency regularization* is a recently-developed technique that encourages smoothness in the learnt decision boundary by requiring minimal shifts in the learnt function when small perturbations are applied to an input sample. This technique has become increasingly common in the state-of-the-art semi-supervised learning [36, 37, 38] and recently for dealing with noisy data [15]. These methods use various complicated pipelines to integrate consistency regularization in training. This work shows that a multi-distribution generalization of JS neatly incorporate such regularization.

Hendrycks *et al.* [6] recently proposed AugMix, a novel data augmentation strategy in combination with a GJS consistency loss to improve uncertainty estimation and robustness to image corruptions at test-time. Our work is orthogonal since we consider the task of learning under noisy labels at training time and conduct corresponding experiments. We also investigate and derive theoretical properties of the proposed loss functions. Finally, our losses are solely implemented based on JS/GJS instead of a combination of CE and GJS in case of AugMix. However, we find it promising that GJS improves robustness to both training-time label noise and test-time image corruption which further strengthens the significance of the JS-based loss functions.

Finally, recently, Xu *et al.* [16]; Wei & Liu [17] propose loss functions with *information theory* motivations. Jensen-Shannon divergence, with inherent information theoretic interpretations, naturally posits a strong connection of our work to those. Especially, the latter is a close *concurrent* work that studies the general family of  $f$ -divergences but takes a different and complementary angle. Reconciling these two works with our study can be, indeed, a fruitful future direction which we consider beyond the scope and limitations of a single work such as ours.